Seismic Resistance of Reinforced Concrete Frame Structures Designed Only for Gravity Loads:

Part I - Design and Properties of a One-Third Scale Model Structure

by

J.M. Bracci[1], A.M. Reinhorn[2] and J.B. Mander[3]

December 1, 1992

Technical Report NCEER-92-0027

NCEER Project Numbers 89-1001A, 90-1001A and 91-3111B

NSF Master Contract Number BCS 90-25010
and
NYSSTF Grant Number NEC-91029

1 Research Associate, Department of Civil Engineering, State University of New York at Buffalo
2 Professor, Department of Civil Engineering, State University of New York at Buffalo
3 Assistant Professor, Department of Civil Engineering, State University of New York at Buffalo

NATIONAL CENTER FOR EARTHQUAKE ENGINEERING RESEARCH
State University of New York at Buffalo
Red Jacket Quadrangle, Buffalo, NY 14261

SECTION 4

IDENTIFICATION OF DYNAMIC CHARACTERISTICS - ELASTIC RESPONSE

4.1 Introduction

The identification of the initial dynamic characteristics of the undamaged model structure are presented first. The characteristics of importance include the following: natural frequencies; modal shapes; equivalent viscous damping ratios; stiffness matrix; and modal participation factors. These characteristics are found through a series of different tests described in Section 3.7.1 using the story displacement and acceleration time history response and frequency domain response of the story transfer functions. Table 4-1 show the testing program for identification of the dynamic characteristics of the undamaged model.

Table 4-1 Identification Testing Program of Model

Test #	Description	Test Label
1	Impact Hammer Test	HAMMER
2	Pull-Back Test	PULL
3	Snap-Back Test	SNAP
4	Compensated White Noise	WHN_B

The theoretical background for determining the dynamic characteristics of a structure from both the experimental time history response and frequency domain story transfer functions is presented. The experimental test results are compared to analytical predictions from STAAD™ (1989). The comparisons and discrepancies among the various tests and analytical predictions are also discussed.

Following the identification of the initial dynamic characteristics of the model, the minor earthquake motion is used to excite the model. This level of excitation is used to identify the elastic (pre-yield) concrete structural properties of the model. The global and local response of the model from this superimposed base motion are presented.

4.2 Identification Procedures

The following derivations show that the natural frequencies, modal shapes, and elastic equivalent viscous damping characteristics of a structure can be determined from the transfer functions of the story acceleration response of the structure and the base motion. Herein, a transfer function is defined as an output structural response normalized by a superimposed input base motion in the frequency domain, (i.e. the Fourier Transform of a story level acceleration time history normalized by the Fourier Transform of the base acceleration time history).

For sake of completeness, the logarithmic-decrement and half-power (bandwidth) methods are also presented for determining the equivalent viscous damping characteristics from the response in the time and frequency domains, respectively.

Next, the stiffness and damping matrices are derived in terms of the mass and orthogonal modal shape matrices.

4.2.1 Frequency Domain Identifications

Modal identifications can be developed from frequency domain analysis procedures. The following describes the identification technique.

4.2.1.1 Modal Shapes

Eq. (4.1) shows the general equation of motion for a multi-degree-of-freedom (MDOF) system excited by a horizontal base acceleration motion, $\ddot{x}_g(t)$.

$$\mathbf{M}\ddot{\mathbf{x}}(t) + \mathbf{C}\dot{\mathbf{x}}(t) + \mathbf{K}\mathbf{x}(t) = -\mathbf{m}\ddot{x}_g(t) \tag{4.1}$$

where $\mathbf{M}$ = Mass matrix of the structure

$\mathbf{C}$ = Viscous damping matrix of the structure

$\mathbf{K}$ = Stiffness matrix of the structure

$\ddot{x}_g(t)$ = Ground (base) acceleration time history

$\mathbf{m} = \mathbf{M} \cdot \bar{\mathbf{I}}$ = Mass vector of the structure

$\bar{\mathbf{I}}$ = Identity vector

$\mathbf{x}(t)$ = Relative story displacement vector time history

$\dot{\mathbf{x}}(t)$ = Relative story velocity vector time history

$\ddot{\mathbf{x}}(t)$ = Relative story acceleration vector time history

The relative story displacement vector, $\mathbf{x}(t)$, can be expressed in modal form by the product of the modal shape matrix, Φ, and modal story displacement vector, $\eta(t)$, of the structure as follows:

$$\mathbf{x}(t) = \Phi \cdot \eta(t) \tag{4.2}$$

Therefore Eq. (4.1) can be expressed in modal form by inserting Eq. (4.2) and the displacement time derivatives as follows:

$$\mathbf{M}\Phi\ddot{\eta}(t) + \mathbf{C}\Phi\dot{\eta}(t) + \mathbf{K}\Phi\eta(t) = -\mathbf{m}\ddot{x}_g(t) \tag{4.3}$$

Multiplying Eq. (4.3) by the transpose of the k-th mode shape, ϕ_k^T, and using modal shape orthogonality properties (discussed in Section 4.2.2), the resulting uncoupled equation of motion for the k-th mode of vibration becomes:

$$M_k^*\ddot{\eta}_k(t) + C_k^*\dot{\eta}_k(t) + K_k^*\eta_k(t) = -\phi_k^T\mathbf{m}\ddot{x}_g(t) \tag{4.4}$$

where $M_k^* = \phi_k^T\mathbf{M}\phi_k$ = k-th modal mass

$C_k^* = \phi_k^T\mathbf{C}\phi_k$ = k-th modal viscous damping

$K_k^* = \phi_k^T\mathbf{K}\phi_k$ = k-th modal stiffness

For convenience, the mode shapes are normalized by the mass matrix such that $M_k^* = 1$ (in Section 4.2.2, it is discussed how this can be accomplished). The results imply that $\Phi_k^T\mathbf{M} = \Phi^{-1}$.

The modal story displacements and displacement time derivatives (velocities and accelerations) for the k-th mode can be transformed into the frequency domain by using the Fourier Transform. The base acceleration can also be converted to the frequency domain in a similar fashion. The resulting equation of motion for the k-th mode in the frequency domain becomes:

$$-\omega^2\eta_k(\omega) + 2i\omega\xi_k\omega_k\eta_k(\omega) + \omega_k^2\eta_k(\omega) = -\Gamma_k\ddot{x}_g(\omega) \tag{4.5}$$

where ω = frequency (rad/sec)

ξ_k = damping ratio for the k-th mode

ω_k = k-th natural frequency (rad/sec)

$\Gamma_k = \phi_k^T\mathbf{m}$ = k-th modal participation factor

Solving Eq. (4.5) for the k-th modal displacement in the frequency domain results in the following:

$$\eta_k(\omega) = \frac{\Gamma_k \cdot \ddot{x}_g(\omega)}{\omega_k^2 - \omega^2 + 2i\omega\xi_k\omega_k} \tag{4.6}$$

The absolute story accelerations, $\ddot{\mathbf{a}}(t)$, can be represented as follows:

$$\ddot{\mathbf{a}}(t) = \ddot{\mathbf{x}}(t) + \ddot{x}_g(t) \tag{4.7}$$

Using Eq. (4.2) and converting to the frequency domain, Eq. (4.7) results in the following:

$$\ddot{\mathbf{a}}(\omega) = -\omega^2\Phi\eta(\omega) + \ddot{x}_g(\omega) \tag{4.8}$$

Premultipling Eq. (4.8) by $\Phi_k^T\mathbf{M}$ results in:

$$\Phi_k^T\mathbf{M}\ddot{\mathbf{a}}(\omega) = -\omega^2\eta(\omega) + \Phi_k^T\mathbf{M}\ddot{x}_g(\omega) \tag{4.9}$$

Define the absolute k-th modal acceleration, $\ddot{\zeta}_k(\omega)$, for each floor as:

$$\ddot{\zeta}_k(\omega) = \Phi_k^T\mathbf{M}\ddot{\mathbf{a}}(\omega) = -\omega^2\eta_k(\omega) + \Gamma_k\ddot{x}_g(\omega) \tag{4.10}$$

Therefore Eq. (4.5) can be represented as:

$$\ddot{\zeta}_k(\omega) + 2i\omega\xi_k\omega_k\eta_k(\omega) + \omega_k^2\eta_k(\omega) = 0 \tag{4.11}$$

Solving for the absolute modal story accelerations for the k-th mode in terms of the modal story displacement in Eq. (4.11) results in the following:

$$\ddot{\zeta}_k(\omega) = -(2i\omega\xi_k\omega_k + \omega_k^2) \cdot \eta_k(\omega) \tag{4.12}$$

Substituting Eq. (4.6) into Eq. (4.12), the absolute modal story accelerations for the k-th mode can be obtained in terms of the base acceleration as follows:

$$\ddot{\zeta}_k(\omega) = \frac{-\Gamma_k \cdot (2i\omega\xi_k\omega_k + \omega_k^2)}{\omega_k^2 - \omega^2 + 2i\omega\xi_k\omega_k} \cdot \ddot{x}_g(\omega) \tag{4.13}$$

Since $\Phi_k^T\mathbf{M} = \Phi^{-1}$ in Eq. (4.10) and considering the superposition of the modes of vibration, the absolute j-th floor acceleration can be expressed as follows:

$$\ddot{a}_j(\omega) = \sum_{k=1}^{n} [\phi_{jk} \cdot \ddot{\zeta}_k(\omega)] \tag{4.14}$$

where $\ddot{a}_j(\omega)$ = j-th floor absolute acceleration

n = modes of vibration

ϕ_{jk} = k-th mass normalized mode shape for the j-th floor (DOF)

Substituting Eq. (4.13) into (4.14), the absolute floor accelerations can be represented as follows:

$$\ddot{a}_j(\omega) = \sum_{k=1}^{n}\left[\frac{-\Gamma_k \cdot (2i\omega\xi_k\omega_k + \omega_k^2)}{\omega_k^2 - \omega^2 + 2i\omega\xi_k\omega_k} \cdot \phi_{jk}\right]\ddot{x}_g(\omega) \tag{4.15}$$

The transfer function is defined as the ratio of a output structural response to a superimposed input base motion in the frequency domain. Therefore, the transfer function for the j-th floor, $\mathbf{H}_j(\omega)$, can be represented by dividing Eq. (4.15) by the input base acceleration, $\ddot{x}_g(\omega)$. Eq. (4.16) shows the resulting transfer function.

$$\mathbf{H}_j(\omega) = \sum_{k=1}^{n} \frac{-\Gamma_k \cdot (2i\omega\xi_k\omega_k + \omega_k^2)}{\omega_k^2 - \omega^2 + 2i\omega\xi_k\omega_k} \cdot \phi_{jk} = \sum_{k=1}^{n} \mathbf{h}_k(\omega) \cdot \phi_{jk} \tag{4.16}$$

However when a structure is lightly damped, the k-th peak magnitude of the j-th floor transfer function occurs very close to the k-th mode natural frequency, thus $\omega = \omega_k$. Also for small damping and well separated modes (narrowbanded systems), the i-th transfer function peak at the k-th natural frequency, $\mathbf{h}_i(\omega_k)$, with resonance at a distant frequency from ω_k, approaches a small value, ε, and can be neglected. Only $\mathbf{h}_k(\omega_k)$, with resonance at ω_k, has a significant value. Therefore the sum in Eq. (4.16) simplifies to the product $\mathbf{h}_k(\omega_k) \cdot \phi_{jk}$. Hence the peak of the j-th transfer function at the k-th natural frequency can be represented as follows:

$$|\mathbf{H}_j(\omega_k)| = \frac{\Gamma_k\sqrt{1+4\xi_k^2}}{2\xi_k} \cdot \phi_{jk} \tag{4.17}$$

Therefore the peak of the j-th transfer function at the k-th natural frequency is proportional to the magnitude of the mass normalized mode shape for the k-th mode and the j-th degree of freedom. The constant of proportionality is a function of the damping ratio and modal participation factor for the k-th mode. Since the constant of proportionality is the same for all degrees of freedom for the k-th mode, the ratio of the peaks in the transfer functions for the different degrees of freedom at the k-th natural frequency are equal to the ratio of the mode shapes for the k-th mode.

The phase angles for the mode shapes are also determined experimentally from the Fourier Transform of the story accelerations as a function of the natural frequencies as follows:

$$\theta(\omega_i) = \tan^{-1}\left(\frac{I(\omega_i)}{R(\omega_i)}\right) \tag{4.18}$$

where $\theta(\omega_i)$ = phase angle for the j-th floor at ω_i

ω_i = i-th natural frequency

$I(\omega_i)$ = imaginary part of the Fourier Ampl. of the j-th story acceleration at ω_i

$R(\omega_i)$ = real part of the Fourier Ampl. of the j-th story acceleration at ω_i

Therefore by comparing the phase angles for each story at the natural frequencies, the mode shape phases can be determined.

4.2.1.2 Damping Characteristics

From Eq. (4.17), the elastic equivalent viscous damping factor for the k-th mode, ξ_k, can be estimated from the experimentally determined j-th story transfer function magnitude, k-th mass normalized mode shape at the j-th DOF, and the k-th modal participation factor as follows:

$$\xi_k = \sqrt{\left[\left(\frac{2\,|\,\mathbf{H}_j(\omega_k)\,|}{\phi_{jk}\Gamma_k}\right)^2 - 4\right]^{-1}} \tag{4.19}$$

The equivalent viscous damping characteristics of an elastic structure can also be determined from a frequency domain response analysis using the well known half-power (bandwidth) method, Clough and Penzien (1975). The k-th mode damping factor is determined from the frequencies at which the response at the k-th natural frequency, ρ_{f_k}, is reduced by $(1/\sqrt{2})$ or frequencies for which the power input is half the input at resonance as shown in Fig. 4-1. Hence the k-th mode viscous damping factor, ξ_k, can be determined by the following:

$$\xi_k = \frac{f_2 - f_1}{f_2 + f_1} = \frac{f_2 - f_1}{2f_k} \tag{4.20}$$

where f_1, f_2 = frequencies when ρ_{f_1}, $\rho_{f_2} = (1/\sqrt{2})\rho_{f_k}$ (See Fig. 4-1)

f_k = k-th natural frequency

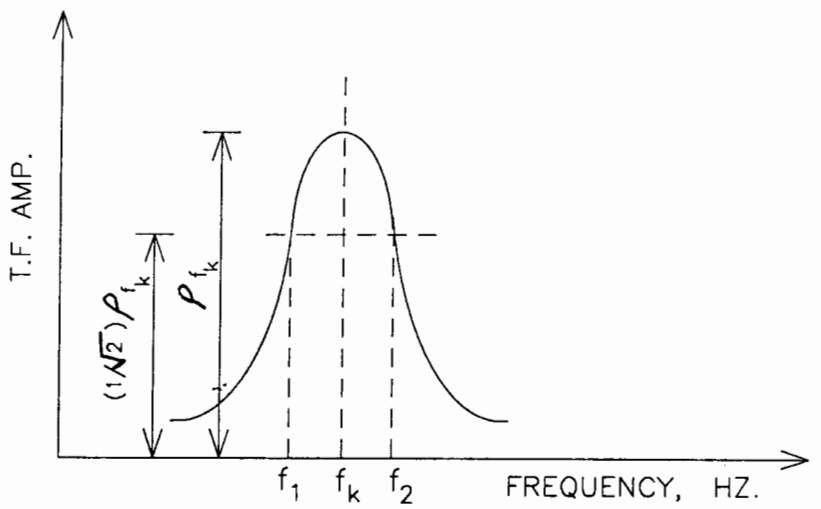

FIG. 4-1 Typical Frequency Response for Determining Damping Characteristics

The equivalent viscous damping characteristics of an elastic SDOF system can also be determined from the decay of a free vibration time history response of the system. From the well known logarithmic decrement method, Craig (1981) and many others, the damping factor, ξ, is estimated by considering peak response which are several cycles apart as follows:

$$\xi = \frac{\ln(v_n / v_{n+m})}{2\pi m} \tag{4.21}$$

where n = Starting cycle
m = arbitrary number of cycles from starting cycle
v_n = Response at cycle n
v_{n+m} = Response at cycle n+m

The free vibration decay method can also be used on the response signals from MDOF systems which are primarily governed by a single mode of vibration, as in a SDOF.

4.2.2 Identification of Structural Stiffness and Damping

A diagonal generalized (modal) mass matrix, $\mathbf{M}_n$, is obtained from the mass and orthogonal modal shape matrices as follows:

$$\mathbf{M}_n = \Phi^T \mathbf{M} \Phi \tag{4.22}$$

where Φ = Modal shape matrix
$\mathbf{M}$ = Mass matrix

The mass normalized modal shape vectors are found by normalizing the i-th mode shape vector by the root of the i-th modal mass, $\phi_{ni} = \phi_i \cdot M_{ni}^{-1/2}$. The normalized modal shape matrix, Φ_n, can then be constructed from the superposition of the normalized modal shape vectors as follows:

$$\Phi_n = [\phi_{n1}, \phi_{n2}, \ldots \phi_{nn}] \tag{4.23}$$

The new generalized mass matrix, developed from the normalized modal shape matrix, has the orthonormal relationship of:

$$\Phi_n^T \mathbf{M} \Phi_n = \mathbf{I} \tag{4.24}$$

where $\mathbf{I}$ = Identity matrix

Using these orthonormal properties, the stiffness matrix, **K**, can be represented as follows:

$$\Phi_n^T \mathbf{K} \Phi_n = \Omega \tag{4.25}$$

where Φ_n = Normalized modal shape matrix

Ω = Diagonal natural frequency matrix $[\omega_1^2, \omega_2^2, \ldots \omega_n^2]$

ω_i = i-th natural frequency (rad/sec)

Therefore the stiffness matrix can be identified as:

$$\mathbf{K} = \Phi_n^{-T} \Omega \Phi_n^{-1} \tag{4.26}$$

From the orthonormal conditions from Eq. (4.24), the following can be derived:

$$\Phi_n^{-T} = \mathbf{M} \Phi_n \tag{4.27a}$$

$$\Phi_n^{-1} = \Phi_n^T \mathbf{M} \tag{4.27b}$$

Therefore substituting Eqs. (4.27a) and (4.27b) into Eq. (4.26) results in the following:

$$\mathbf{K} = \mathbf{M} \Phi_n \Omega \Phi_n^T \mathbf{M} \tag{4.28}$$

Therefore Eq. (4.28) is used to identify the stiffness matrix of a structure from the known mass matrix, experimentally determined natural frequencies, and orthonormal modal shape matrix.

For a typical shear-type building with lumped story level masses and rigid floors, the stiffness matrix can be described as follows:

$$\mathbf{K} = \begin{pmatrix} k_3 & -k_3 & 0 \\ -k_3 & k_2 + k_3 & -k_2 \\ 0 & -k_2 & k_1 + k_2 \end{pmatrix} \tag{4.29}$$

where k_i = i-th story stiffness

A comparison of these story stiffnesses is observed throughout the testing of the model structure for deterioration.

The damping matrix can be developed by assuming proportional damping with the same theory as the stiffness matrix determination as follows:

$$\mathbf{C} = \mathbf{M}\Phi_n\zeta\Phi_n^T\mathbf{M} \tag{4.30}$$

where ζ = Diagonal matrix $[2\xi_1\omega_1, 2\xi_2\omega_2, \ldots 2\xi_n\omega_n]$

ξ_i = i-th mode damping ratio

ω_i = i-th natural frequency (rad/sec)

4.2.3 Internal Energy Quantification

The energy equation for a N-story building subjected to a base motion was derived by Uang and Bertero (1990) as follows:

$$\frac{1}{2}\dot{\mathbf{v}}_t^T\mathbf{M}\dot{\mathbf{v}}_t + \int \mathbf{f}_d^T d\mathbf{v} + \int \mathbf{f}_s^T d\mathbf{v} = \int\left(\sum_{i=1}^{N} m_i\ddot{v}_{ti}\right)dv_g \tag{4.31}$$

where $\mathbf{M}$ = diagonal mass matrix

$\dot{\mathbf{v}}_t$ = absolute velocity vector

$\mathbf{v}$ = relative displacement vector

$\mathbf{f}_d$ = damping force vector

$\mathbf{f}_s$ = restoring force vector

m_i = lumped mass of the i-th floor

$\ddot{v}_{ti}$ = absolute acceleration at the i-th floor

v_g = ground displacement

The kinetic energy, E_K, of a N-story building is calculated from the summation of the kinetic energy at each floor level as follows:

$$E_K = \frac{1}{2}\dot{\mathbf{v}}_t^T \mathbf{M} \dot{\mathbf{v}}_t = \frac{1}{2}\sum_{i=1}^{N} m_i (\dot{v}_{ti})^2 \tag{4.32}$$

where $\dot{v}_{ti}$ = absolute velocity at the i-th floor

The input energy, E_I, to the N-story building is calculated from the summation of the work done by the inertia forces ($m_i \ddot{v}_{ti}$) at each floor for the superimposed ground displacement as follows:

$$E_I = \int \left(\sum_{i=1}^{N} m_i \ddot{v}_{ti} \right) dv_g \tag{4.33}$$

Note that the summation of the inertia forces at each floor is the induced base shear force on the structure.

The energy absorbed by the restoring forces, E_A, can be resolved into the irrecoverable hysteretic (dissipated) energy, E_H, and recoverable elastic strain energy, E_S, as follows:

$$E_A = \int \mathbf{f}_s^T d\mathbf{v} = E_S + E_H \tag{4.34}$$

where

$$E_S = \sum_{i=1}^{N} \frac{V_i^2}{2K_i}$$

$$E_H = \sum_{i=1}^{N} \int V_i d\delta_i - \sum_{i=1}^{N} \frac{V_i^2}{2K_i}$$

V_i = undamped story shear force history

K_i = unloading stiffness of the story shear versus inter-story drift history

δ_i = inter-story drift history

Therefore the viscous damped energy, E_D, can be determined as follows:

$$E_D = \int \mathbf{f}_d^T d\mathbf{v} = E_I - E_K - E_H - E_S \tag{4.35}$$

However note that the experimentally recorded story shear forces include the effects of the equivalent viscous damping present. Therefore the absorbed/dissipated hysteretic and viscous damped energies will be lumped together in the experimental study.

4.3 Experimental Results

The order of the test response results for identification of the initial dynamic characteristics of the model are in accordance with Table 4-1.

4.3.1 Impact Hammer Test

After the unloaded three story model was lifted and secured to the shaking table, an impact hammer (test label - HAMMER) was used to excite the model for identification of the dynamic characteristics of the unloaded (bare) model. Since an impact hammer can only provide a low magnitude of excitation with each strike, an average of five hammer strikes on the third story of the model was used for determination of the story transfer functions. Fig. 4-2 shows the average transfer functions from a spectrum analyzer for the first (4.2c), second (4.2b), and third (4.2a) stories in the frequency domain from hammer strikes to the third floor. The definition and application of transfer functions are discussed in the identification procedures (Section 4.2).

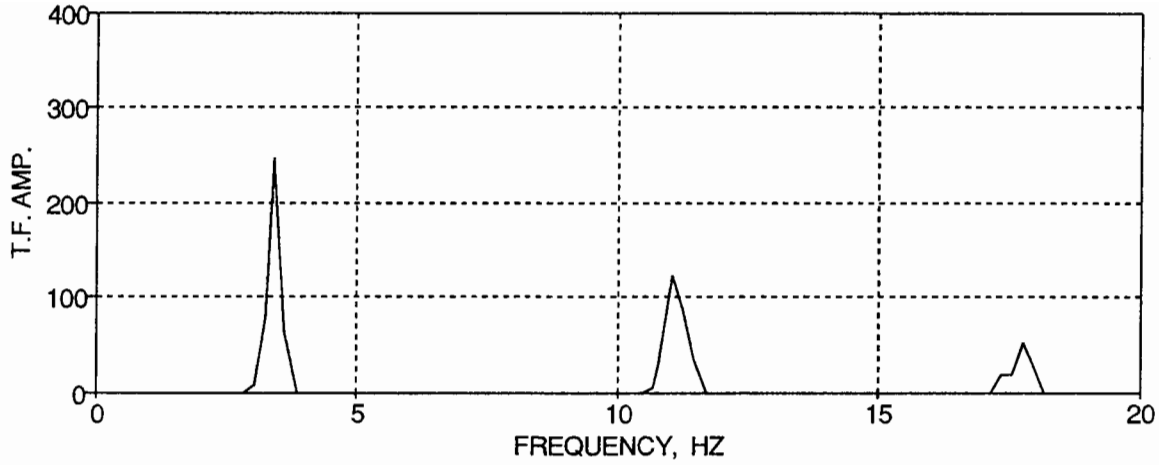

(a) First Floor

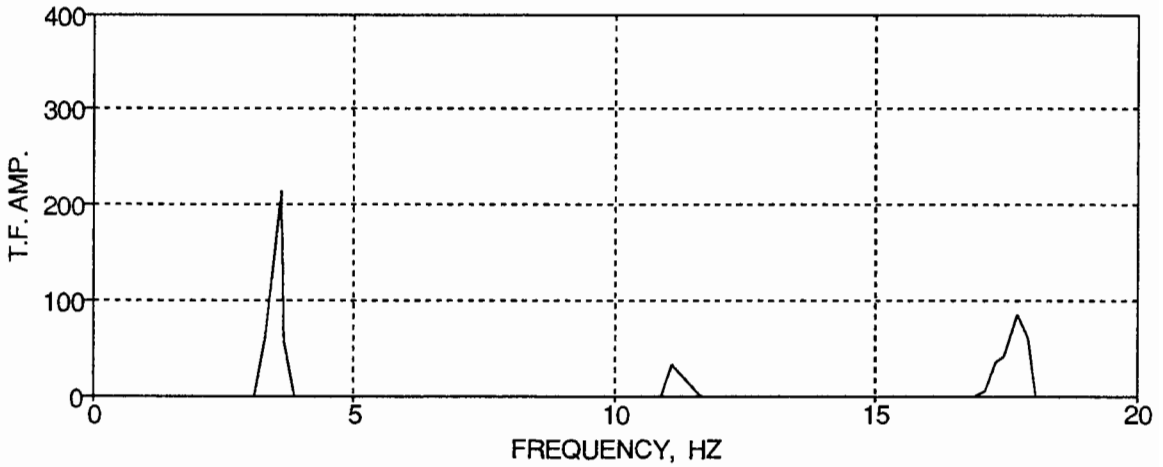

(b) Second Floor

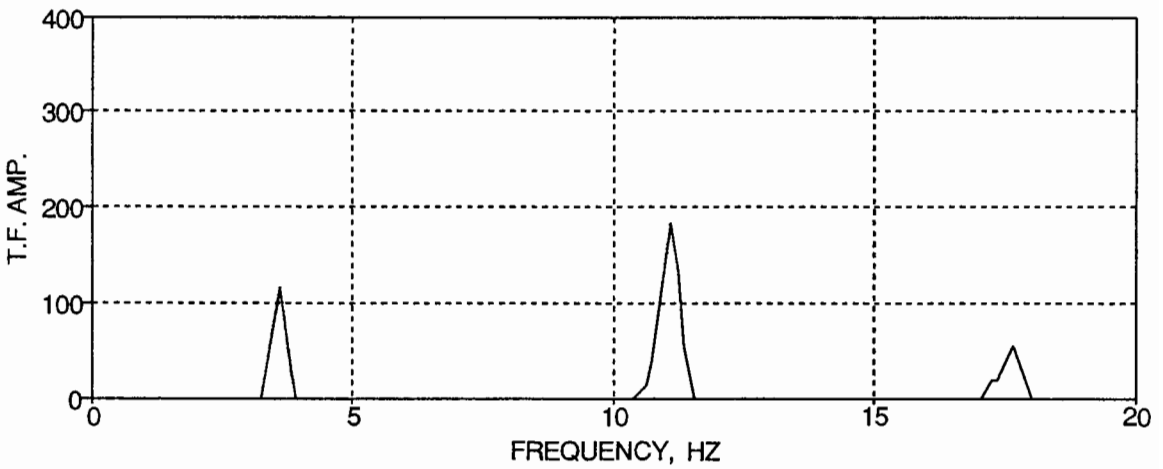

(c) Third Floor

FIG. 4-2 Story Transfer Functions from an Impact Hammer Test

4.3.2 Pull-Back Tests

Once the additional balast weights were loaded on the model for mass similitude, a measured flexibility matrix ($\mathbf{F}_{ij}$) of the loaded model, Eq. (4.36), was obtained by statically loading the center of the bay for each floor with horizontal tensile loads of about 0.5 and 1.0 kips (test label - PULL) and recording story displacements at the east and west floor-slab levels with the displacement transducers (D3 - D8). Fig. 4-3 shows a detail of the horizontal tensile loading and displacement measurement locations on the model. The coefficients of the flexibility matrix are then determined based on an average of four displacement readings for each story loading, two displacement readings for each horizontal story load.

$$\mathbf{F}_{ij} = \begin{pmatrix} 7.18 & 4.77 & 2.33 \\ 4.64 & 4.36 & 2.18 \\ 2.20 & 2.13 & 1.95 \end{pmatrix} \times 10^{-2} \text{ in/kip} = \begin{pmatrix} f_{III,III} & f_{III,II} & f_{III,I} \\ f_{II,III} & f_{II,II} & f_{II,I} \\ f_{I,III} & f_{I,II} & f_{I,I} \end{pmatrix} \tag{4.36}$$

where i = floor displacement location

j = floor pull location

I,II,III = first, second, and third floors, respectively

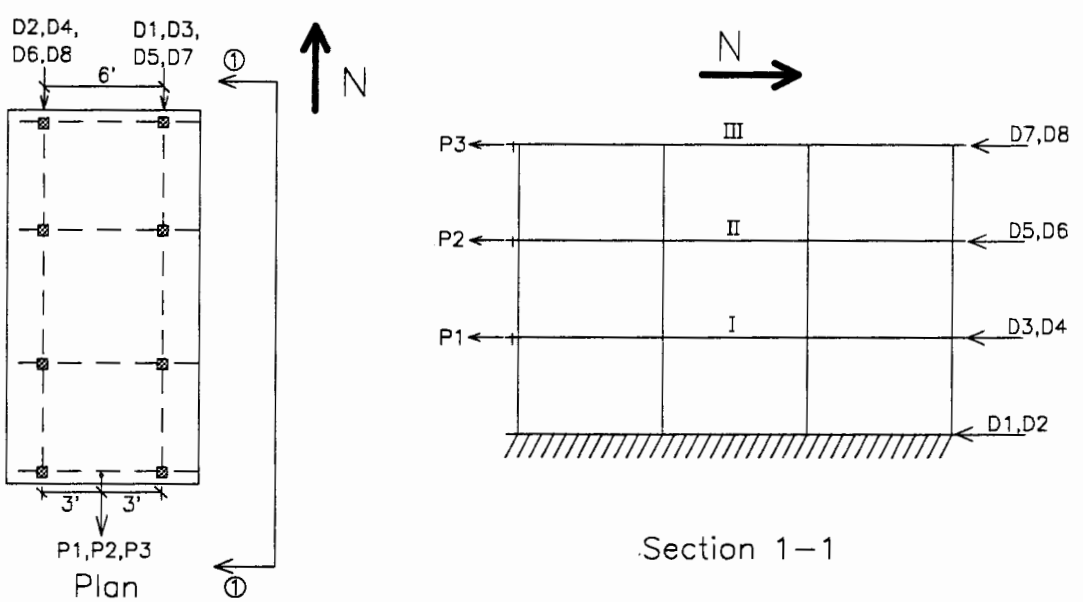

FIG. 4-3 Pull-Back Loading and Displacement Measurement Locations

4.3.3 Snap-Back Tests

Quick release (snap-back) tests were next performed on the loaded model (test label - SNAP). Each floor of the model is statically loaded with a horizontal tensile force of about 1.0 kip (same locations as test PULL, see Fig. 4-3) and quickly released (snapped) permitting the model to vibrate freely. Fig. 4-4 shows the third story displacement time history response (displacement transducer D7) from a third floor snap. It can be observed that a static displacement of 0.083 in. is produced from a horizontal tensile load of about 1.1 kips. The story level horizontal acceleration response are recorded through the accelerometers (AH3 - AH8). Fig. 4-5 shows the acceleration response time history for each floor of the model when that floor is snapped.

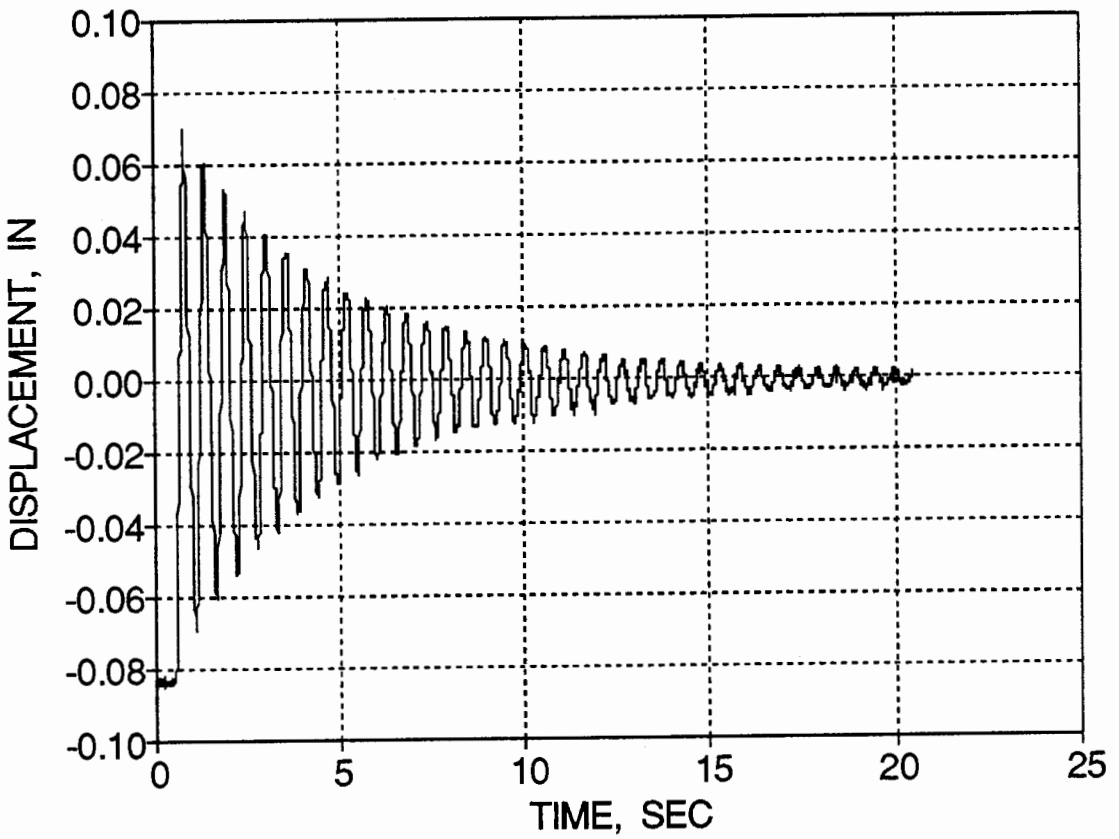

FIG. 4-4 Third Story Displacement Response from a Third Floor Snap

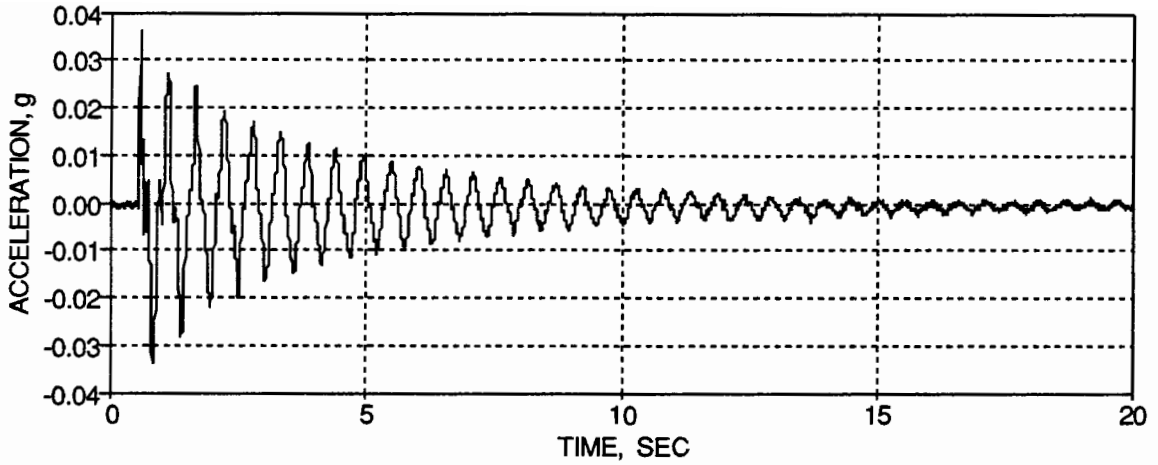

(a) Third Floor

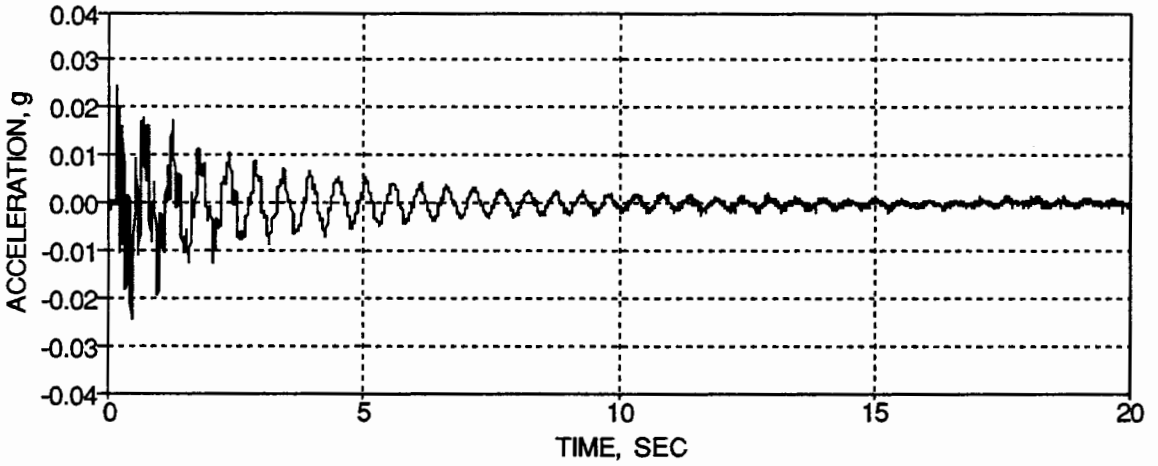

(b) Second Floor

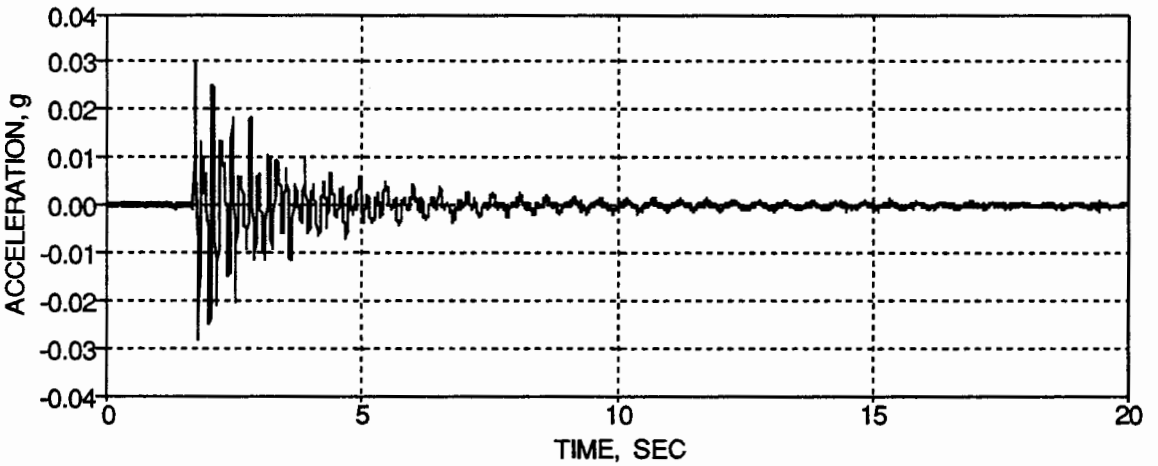

(c) First Floor

FIG. 4-5 Acceleration Story Response from that Story Snap

4.3.4 White Noise Test

The first motion of the shaking table that was used to excite the loaded model, including the wood safety frames, was a wide banded frequency response (0 - 50 Hz.) white noise excitation, test label WHN_A. This white noise test was used for proper calibration of the shaking table. After the shaking table was recalibrated, a compensated white noise excitation, WHN_B, was derived and used for the identification of the initial dynamic characteristics of the model. Fig. 4-6 shows the base acceleration motion of the shaking table for the white noise excitation WHN_B. The peak acceleration of the base can be observed as about 0.024 g. The story level acceleration response from WHN_B are shown in Fig. 4-7.

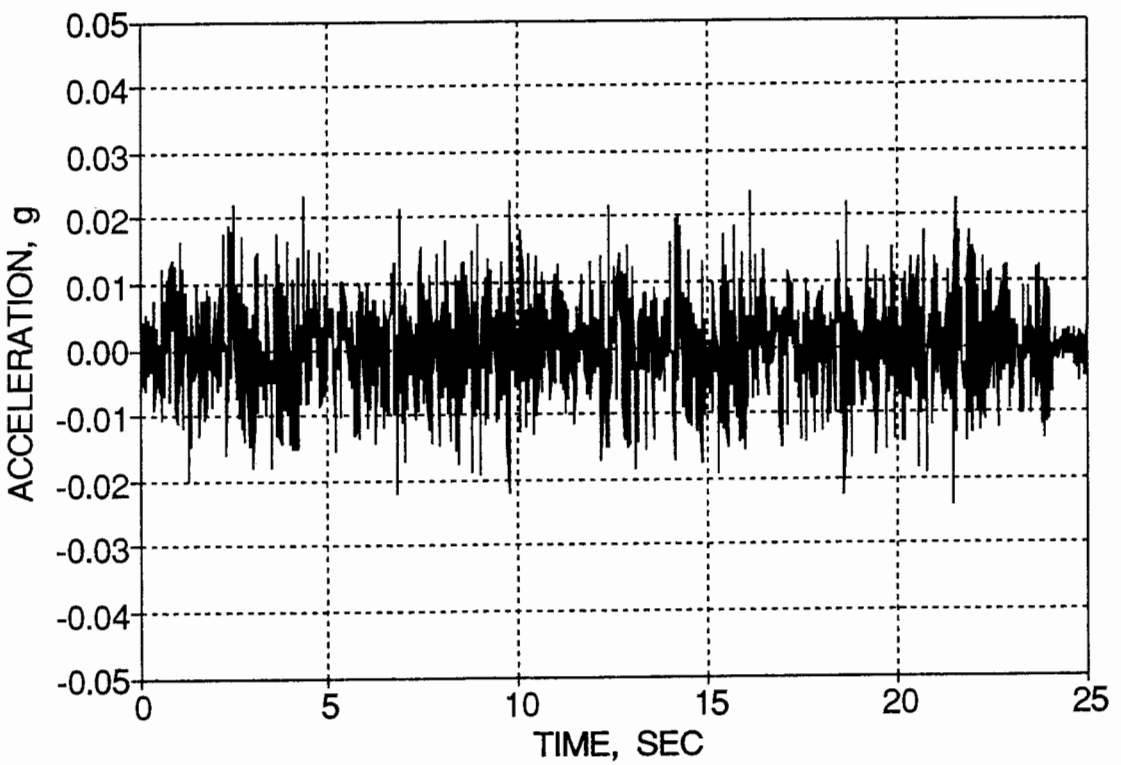

FIG. 4-6 Base Acceleration Motion of the White Noise Excitation, WHN_B

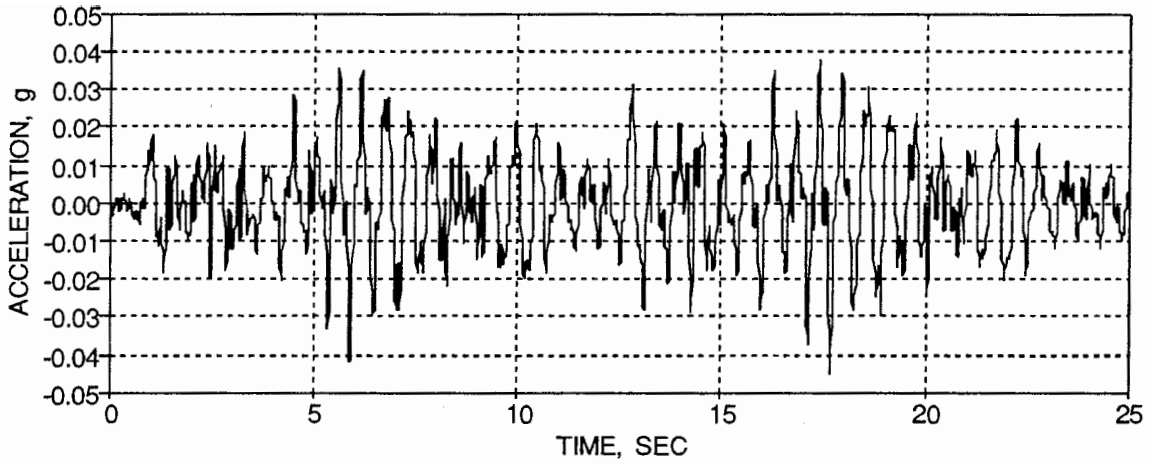

(a) Third Floor

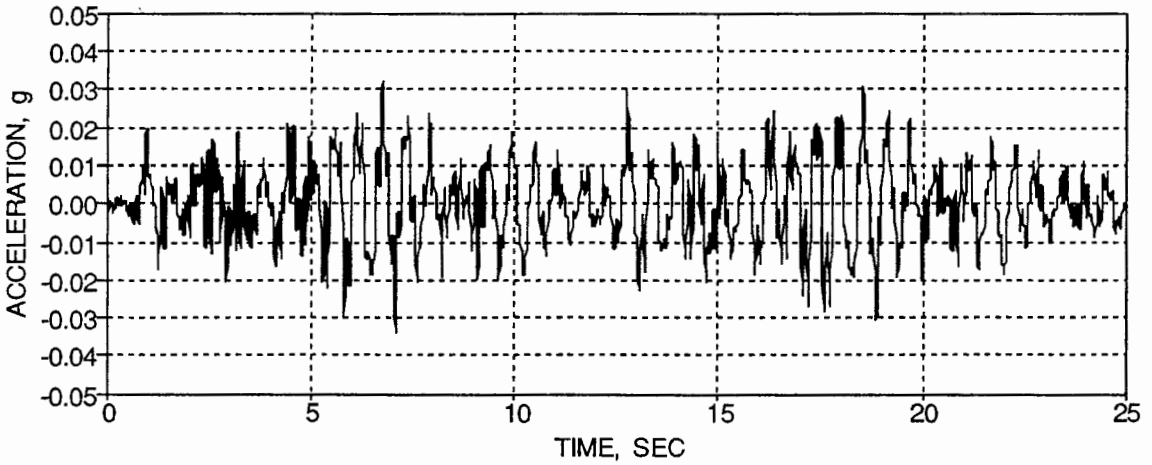

(b) Second Floor

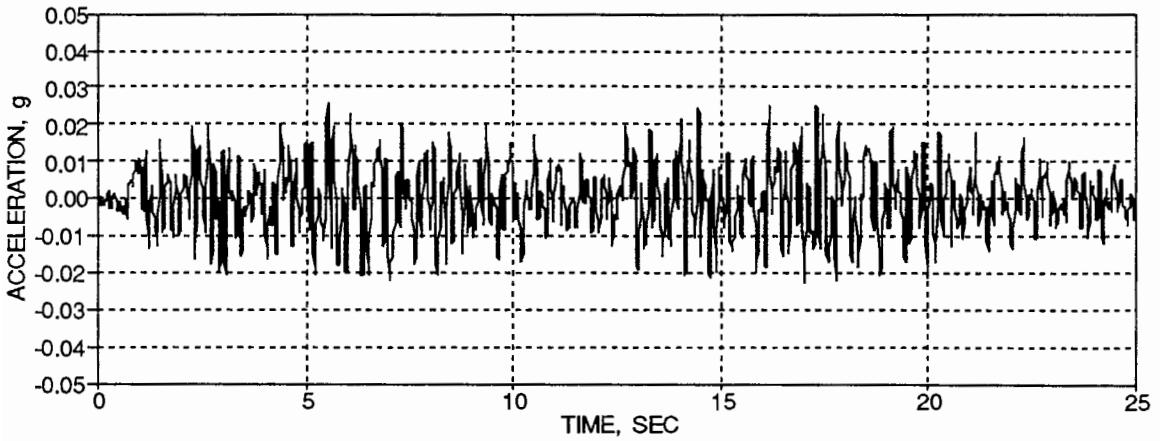

(c) First Floor

FIG. 4-7 Story Level Acceleration Response from WHN_B

4.4 Dynamic Characteristics of Model

A complete list of the identified natural frequencies and equivalent viscous damping characteristics of the unloaded and loaded model from the following tests are presented in Tables 4-2 and 4-3, respectively. The identified modal shapes, stiffness, and viscous damping matrices are presented in Tables 4-4 through 4-8, respectively.

4.4.1 Properties of Unloaded Model - Impact Hammer Test

Since the story transfer functions have small damping and well separated modes (see Fig. 4-2), the assumptions made in the development of the previous section are justified. Therefore, the peaks occur precisely at the natural frequencies of the unloaded model, $\mathbf{f}_i^u$, and are identified as follows:

$$\mathbf{f}_i^u = \begin{pmatrix} 3.40 \\ 11.00 \\ 17.60 \end{pmatrix} Hz. \tag{4.37}$$

where i = mode of vibration

Since the story transfer functions have small damping and well separated modes, the ratio of the story transfer function magnitudes at the k-th natural frequency is equal to the ratio of the k-th mode shape. From the phase angles of the story transfer functions at each natural frequency, the modal shape matrix, Φ_{ij}^u, for the unloaded model is identified as shown below:

$$\Phi_{ij}^u = \begin{pmatrix} 1.00 & -0.67 & -0.62 \\ 0.82 & 0.18 & 1.00 \\ 0.47 & 1.00 & -0.63 \end{pmatrix} = \begin{pmatrix} \phi_{III,1} & \phi_{III,2} & \phi_{III,3} \\ \phi_{II,1} & \phi_{II,2} & \phi_{II,3} \\ \phi_{I,1} & \phi_{I,2} & \phi_{I,3} \end{pmatrix} \tag{4.38}$$

where i = degree of freedom, where i = III being the third floor
j = mode of vibration

The equivalent viscous damping factors of the unloaded model are estimated using the half-power (bandwidth) method, Eq. (4.20), from the story transfer functions as 2.7%, 1.5%, and 1.0%, respectively.

Based on an estimated quantities presented in Section 3.5, the mass matrix for the unloaded for mass similitude model, $\mathbf{M}_{ij}^{u}$, is shown below:

$$\mathbf{M}_{ij}^{u} = \begin{pmatrix} 0.0162 & 0.0000 & 0.0000 \\ 0.0000 & 0.0162 & 0.0000 \\ 0.0000 & 0.0000 & 0.0162 \end{pmatrix} \text{ kip/in/sec}^2 \tag{4.39}$$

The stiffness matrix of the unloaded model, $\mathbf{K}_{ij}^{u}$, is identified using Eq. (4.28) and shown below:

$$\mathbf{K}_{ij}^{u} = \begin{pmatrix} 70.1 & -72.1 & 10.3 \\ -72.1 & 115.5 & -59.2 \\ 10.3 & -59.2 & 97.3 \end{pmatrix} \text{ kip/in} \tag{4.40}$$

The story stiffnesses of the unloaded model, defined in Eq. (4.29), are identified using Eq. (4.40) and shown below:

$$\mathbf{k}_{i}^{u} = \begin{pmatrix} 72.1 \\ 59.2 \\ 38.1 \end{pmatrix} \text{ kip/in} \tag{4.41}$$

Similarly, the damping matrix of the unloaded model was identified using Eq. (4.30) and shown below:

$$\mathbf{C}_{ij}^{u} = \begin{pmatrix} 0.028 & -0.007 & -0.003 \\ -0.007 & 0.028 & -0.005 \\ -0.003 & -0.005 & 0.033 \end{pmatrix} \text{ kip-sec/in} \tag{4.42}$$

4.4.2 Properties of Loaded Model - Pull-Back Tests

Pull-back tests were performed on the loaded model to obtain the flexibility matrix and indirectly the stiffness matrix. The minor lack of symmetry in the off-diagonal terms of the measured flexibility matrix, Eq. (4.36), is primarily due to the averaging in determining the matrix and experimental errors in the instrumentation for small loadings and displacements. The modulus of elasticity of a R/C member is also nonlinearly a function of the magnitude of the displacement (strain). Therefore deviations in the flexibility matrix are also expected from the low amplitude story displacements for the pull-back tests. For analytical evaluations, a symmetric flexibility matrix, $\overline{\mathbf{F}}_{ij}$, and an "error" matrix, $\mathbf{E}_{ij}$, are determined by averaging the off-diagonal terms from Eq. (4.36) and are shown in Eq. (4.43a) and (4.43b).

$$\mathbf{F}_{ij} = \overline{\mathbf{F}}_{ij} + \mathbf{E}_{ij} \tag{4.43a}$$

$$\mathbf{F}_{ij} = \begin{pmatrix} 7.18 & 4.70 & 2.27 \\ 4.70 & 4.36 & 2.16 \\ 2.27 & 2.16 & 1.95 \end{pmatrix} + \begin{pmatrix} 0.00 & -0.07 & -0.07 \\ 0.07 & 0.00 & -0.03 \\ 0.07 & 0.03 & 0.00 \end{pmatrix} \text{ x } 10^{-2} \text{ in/kip} \tag{4.43b}$$

Inverting the symmetric flexibility matrix for the model, $\overline{\mathbf{F}}_{ij}$, from Eq. (4.43b) results in a measured stiffness matrix, $\mathbf{K}_{ij}$, as shown below:

$$\mathbf{K}_{ij} = \begin{pmatrix} 47.4 & -52.7 & 3.2 \\ -52.7 & 109.3 & -59.8 \\ 3.2 & -59.8 & 113.9 \end{pmatrix} \text{ kip/in} \tag{4.44}$$

The story stiffnesses of the loaded model, defined in Eq. (4.29), are identified from Eq. (4.44) and shown below:

$$\mathbf{k}_i = \begin{pmatrix} 52.7 \\ 59.8 \\ 54.1 \end{pmatrix} \text{ kip/in} \tag{4.45}$$

Based on an estimated quantities presented in Section 3.5, the mass matrix for the loaded model, $\mathbf{M}_{ij}$, is shown below:

$$\mathbf{M}_{ij} = \begin{pmatrix} 0.070 & 0.000 & 0.000 \\ 0.000 & 0.070 & 0.000 \\ 0.000 & 0.000 & 0.070 \end{pmatrix} \text{ kip/in/sec}^2 \tag{4.46}$$

From an eigenvalue (free vibration) analysis for a lightly damped system, the circular natural frequencies, ω_i , are determined by equating the determinant of $[\mathbf{K}_{ij} - \mathbf{M}_{ij}\omega_i^2]$ to zero. The natural frequencies, $\mathbf{f}_i$, are thus identified as:

$$\mathbf{f}_i = \begin{pmatrix} 1.76 \\ 5.34 \\ 8.15 \end{pmatrix} \text{ Hz.} \tag{4.47}$$

The mode shapes of the model are also determined from the eigenvalue analysis by equating $[\mathbf{K}_{ij} - \mathbf{M}_{ij}\omega_i^2]\phi_i$ to zero for each mode i, where ϕ_i is the i-th vector mode shape. By assembling these mode shapes, the modal shape matrix is identified as follows:

$$\Phi_{ij} = \begin{pmatrix} 1.00 & -0.82 & -0.41 \\ 0.76 & 0.55 & 1.00 \\ 0.40 & 1.00 & -0.88 \end{pmatrix} \tag{4.48}$$

4.4.3 Properties of Loaded Model - Quick Release (Snap-Back) Free Vibration Tests

Each floor of the model was statically loaded and then quickly released (snapped) to create free vibrations of the model. Based on the floor snapped, the Fourier Transform of the acceleration response of that story from Fig. 4-5 are shown in Fig. 4-8. Again for small damping and well separated modes (see Fig. 4-8), the peaks in the Fourier Transform occur precisely at the natural frequencies of the model, just as in a transfer function. Thus the natural frequencies of the model are identified as:

$$\mathbf{f}_i = \begin{pmatrix} 1.86 \\ 5.66 \\ 8.40 \end{pmatrix} \text{ Hz.} \tag{4.49}$$

Fig. 4-8a shows that the third floor acceleration frequency response from a third floor snap is primarily governed by the first mode of vibration (since the peak response amplitude at the first mode natural frequency is much greater than the peak response amplitudes at the second and third mode natural frequencies). Hence from the third floor free vibration acceleration response time history, shown in Fig. 4-5a, the first mode equivalent viscous damping factor is determined to be 2.5% using the logarithmic decrement method, Eq. (4.21).

The second and third mode damping factors are determined from the logarithmic decrement method for each mode after the time functions are filtered in the frequency domain. The filtered Fourier Transforms are determined by the product of the Fourier Amplitudes and the step functions, $u_i(f)$, shown in Eq. (4.50a) and (4.50b), respectively.

$$u_2(f) = \begin{Bmatrix} 1.0 & \text{when} & 2.93Hz. \le f \le 7.23Hz. \\ 0.0 & \text{when} & f < 2.93Hz. \text{ or } f > 7.23Hz. \end{Bmatrix} \tag{4.50a}$$

$$u_3(f) = \begin{Bmatrix} 1.0 & \text{when} & 7.28Hz. \le f \le 11.04Hz. \\ 0.0 & \text{when} & f < 7.28Hz. \text{ or } f > 11.04Hz. \end{Bmatrix} \tag{4.50b}$$

where f = frequency (Hz.)

Then these filtered Fourier Transforms for the second and third modes are multiplied by a normalized Gaussian window or function $g(f)$, shown in Eq. (4.51), to lessen the effect of the frequencies away from the natural frequency of that mode and thereby reduce the noise in the signal and leakage in the transform.

$$g(f) = \frac{1}{\sqrt{2\pi}\sigma} e^{-(f-\bar{f})/2\sigma^2}, \quad -\infty < f < \infty \tag{4.51}$$

where $\bar{f}$ = resonant natural frequency, 5.56 Hz. and 8.30 Hz., respectively

σ = variable standard deviations of 18.6% and 13.3% of the frequency range, respectively

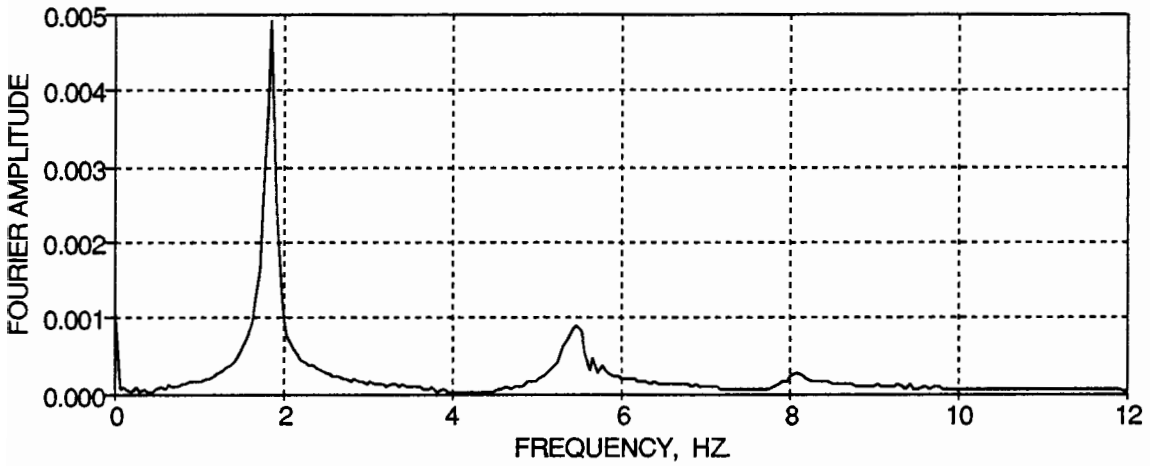

(a) Third Floor

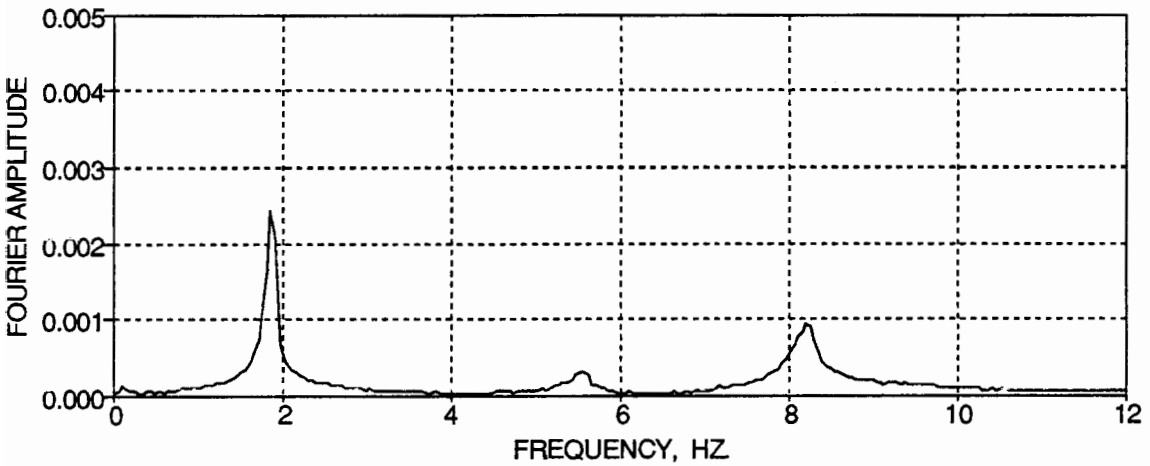

(b) Second Floor

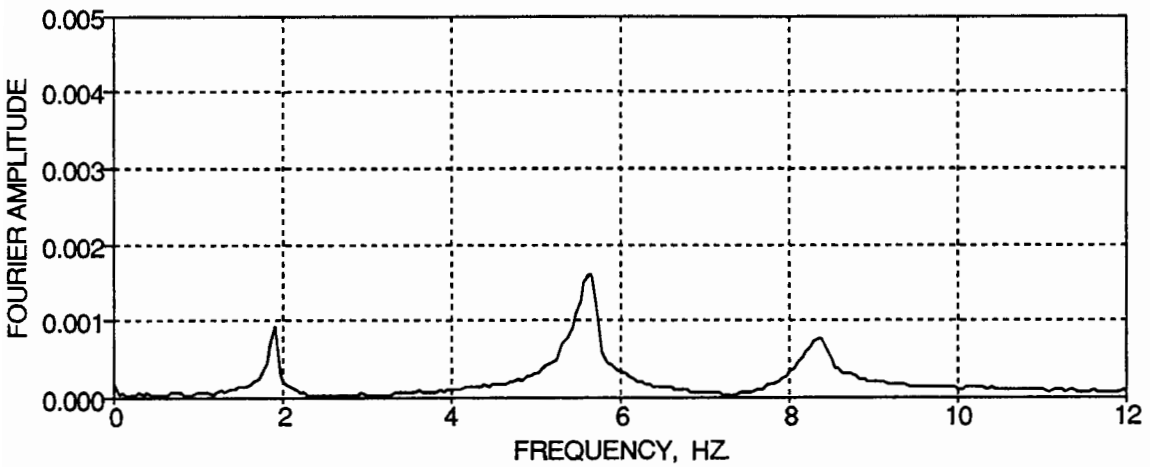

(c) First Floor

FIG. 4-8 Fourier Transform of the Story Level Accelerations from the Snap-Back Tests

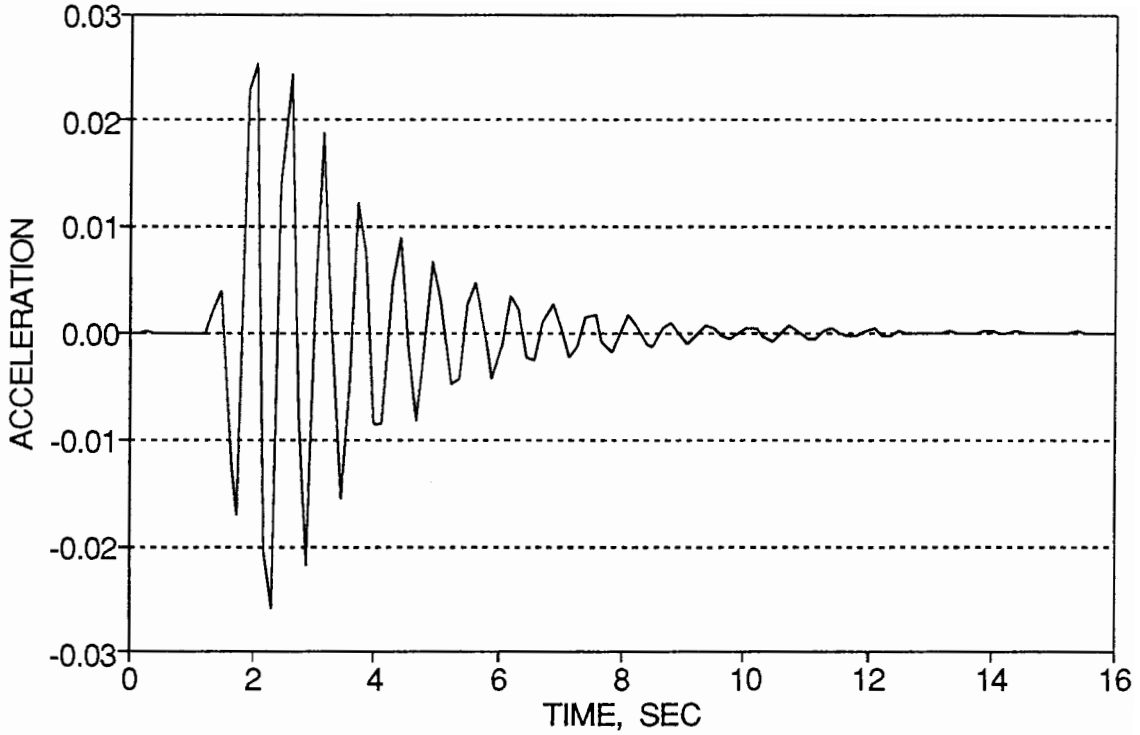

(a) Second Mode

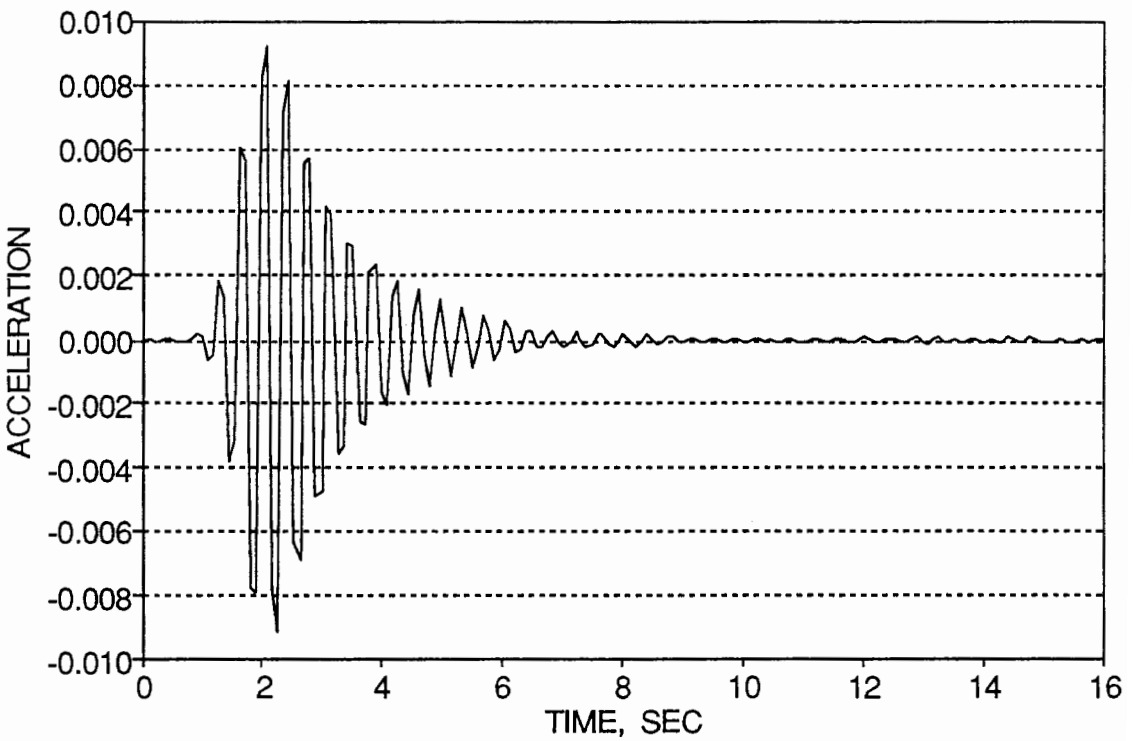

(b) Third Mode

FIG. 4-9 Inverse Fourier Transform of Filtered Frequencies

The inverse Fourier Transforms (time domain response) for the second and third modes of vibration are shown in Fig. 4-9a and 4.9b, respectively. The damping factors for these modes are then determined from Eq. (4.21) as 4.8% and 4.0%, respectively.

4.4.4 Properties of Loaded Model - Initial White Noise Excitation on Shaking Table

A white noise shaking table excitation was also used to determine the dynamic characteristics of the model. Fig. 4-10a shows the Fourier Transform of the input white noise base acceleration motion from Fig. 4-6 and Fig. 4-10b shows the smoothed signal using a moving average of 7 digital points to reduce the noise. A wide banded excitation in the frequency domain is observed.

The story transfer functions, comprised of the Fourier Amplitudes of the story level accelerations from Fig. 4-7 normalized by the Fourier Amplitudes of the input base motion in Fig. 4-10, are shown in Fig. 4-11. It can be observed that the transfer functions near the second and third mode natural frequencies have several sharp peaks or dominant frequencies. This phenomenon developed due to the non-linear behavior of the cracked reinforced concrete members from the white noise excitation. The cracking creates a stick-slip type condition causing excitation of several frequencies near the second and third natural frequencies. The transfer functions near the first natural frequency shows only one clear dominant frequency. Therefore, the influence of cracking does not appear to affect the structural response in this mode during this input excitation.

Since transfer functions for inelastic (non-linear) behavior in R/C members have many peaks near a mode of vibration as opposed to an elastic system with only one clear dominant frequency, the modal natural frequencies are identified through an average procedure for that mode. This is accomplished by smoothing the transfer function using a moving average of every 3 digital points in the signal. Fig. 4-12 shows the resulting smoothed transfer functions for WHN_B. Therefore the average modal natural frequencies are thus identified as:

$$\mathbf{f}_i = \begin{pmatrix} 1.78 \\ 5.32 \\ 7.89 \end{pmatrix} \text{ Hz.} \tag{4.52}$$

Since the transfer functions again have small damping and well separated modes (see Figs. 4-11 and 4-12), the modal shape matrix, Eq. (4.53), is thus determined from the ratio of the transfer function magnitudes for each floor at each natural frequency and the comparison of phase angles at each natural frequency for each degree-of-freedom.

$$\Phi_{ij} = \begin{pmatrix} 1.00 & -0.82 & -0.46 \\ 0.80 & 0.46 & 1.00 \\ 0.42 & 1.00 & -0.83 \end{pmatrix} \tag{4.53}$$

Some smoothing techniques result in considerable drops in the response amplitudes of the transfer functions. And since the half-power method considers the response amplitude at a certain frequency, equivalent viscous damping identifications could be distorted. But it can be observed in Fig. 4-12 that the smoothing technique presented results in minor drops in the peak magnitudes of the transfer functions. Therefore the equivalent viscous modal damping factors are determined through the half-power (bandwidth) method from the smoothed transfer functions for each story (Fig. 4-12) as 2.0%, 2.4%, and 2.0%, respectively and are shown in Table 4-3. By considering the wide range of dominant frequencies (near the second natural frequency), the second mode damping factor is observed to be slightly higher than for the other modes. Some contributions of hysteretic damping may have occurred for this mode due to the cracking in the members of the model, accompanied by slight shifts of frequencies (stiffness changes).

The estimated viscous damping factors are also found from the transfer functions using Eq. (4.19) as 1.7%, 1.6%, and 1.4% for the first, second, and third modes, respectively. Take note that the damping factors were calculated based on the smoothed story transfer functions to account for the high frequency noise in the signal.

From the orthogonal modal shape matrix in Eq. (4.53), the stiffness matrix is derived using Eq. (4.28) and is shown below:

$$\mathbf{K}_{ij} = \begin{pmatrix} 51.9 & -53.4 & 2.5 \\ -53.4 & 102.4 & -54.4 \\ 2.5 & -54.4 & 104.7 \end{pmatrix} \text{ kip/in} \tag{4.54}$$

The story stiffnesses of the loaded model, defined in Eq. (4.29), are identified from Eq. (4.54) and shown below:

$$\mathbf{k}_i = \begin{pmatrix} 53.4 \\ 54.4 \\ 50.3 \end{pmatrix} \text{ kip/in} \tag{4.55}$$

Similarly, the damping matrix is derived from Eq. (4.30) and is shown below:

$$\mathbf{C}_{ij} = \begin{pmatrix} 0.072 & -0.042 & -0.012 \\ -0.042 & 0.097 & -0.029 \\ -0.012 & -0.029 & 0.112 \end{pmatrix} \text{ kip-sec/in} \tag{4.56}$$

The initial modal participation factors, Γ_k, are determined from the results of the white noise test using the derivations in Section 4.2.1.1 as:

$$\Gamma_k = \begin{pmatrix} 0.44 \\ 0.12 \\ -0.06 \end{pmatrix} \tag{4.57}$$

Fig. 4-13 shows the story shear versus inter-story drift histories for WHN_B. The initial stiffnesses from these histories are identified as 51.2 kip/in, 42.2 kip/in, and 40.0 kip/in, respectively. It can also be observed that loops occurred in these histories. Although it is important to note that these loops are not a result of inelastic hysteresis but from the equivalent viscous damping from the cracked R/C members of the structure. Therefore the story shears and drifts recorded through the instrumentation includes the effects of viscous damping as stated previously. For the following experimental white noise excitations, a comparison of these initial stiffnesses are examined for correlating the stiffness degradation in the structure.

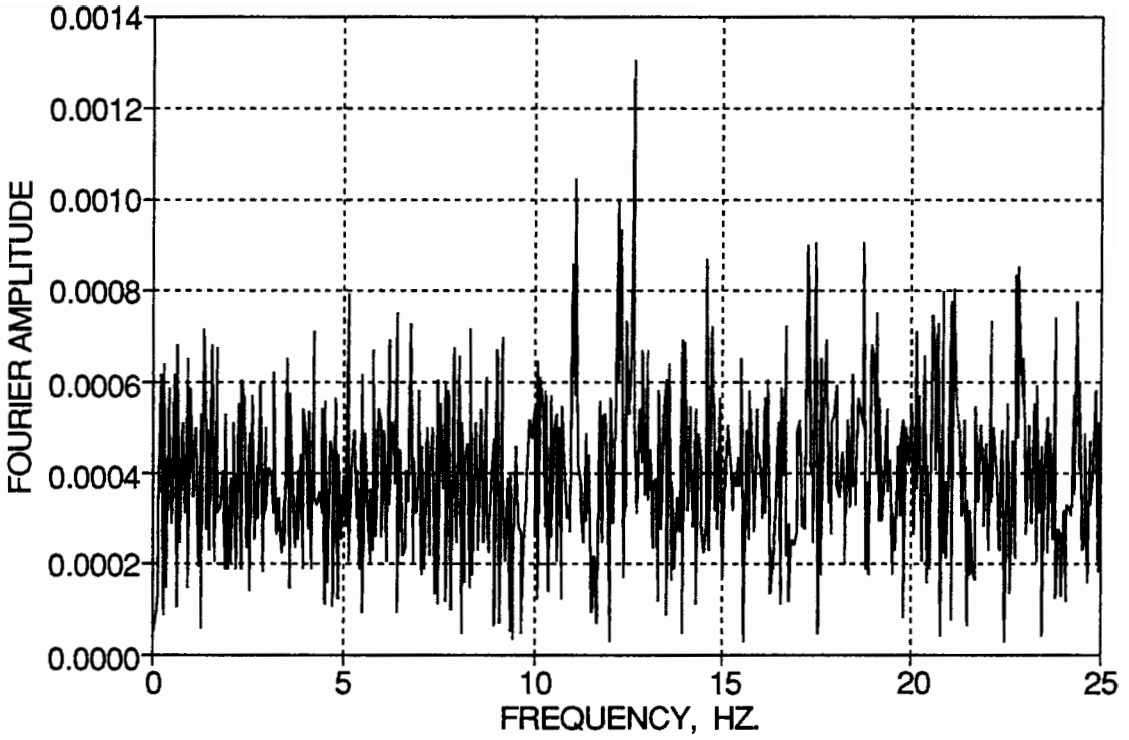

(a) Fourier Transform

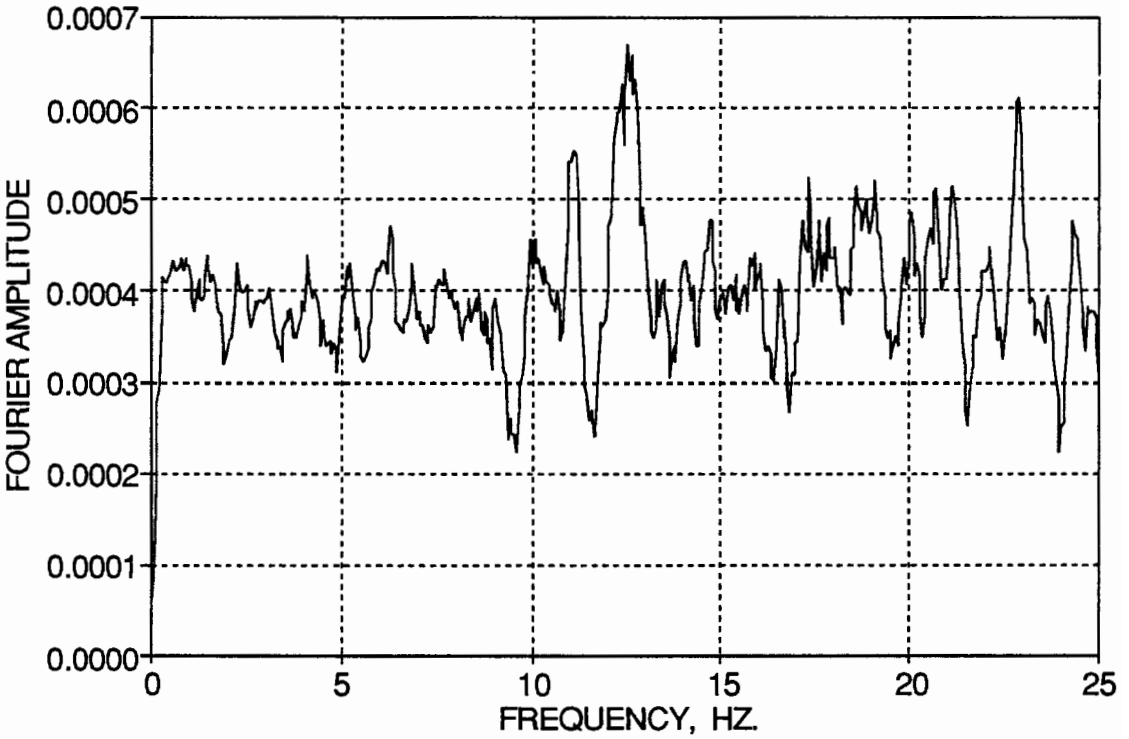

(b) Smoothed Fourier Transform

FIG. 4-10 Fourier Transform of the Base Acceleration Motion for WHN_B

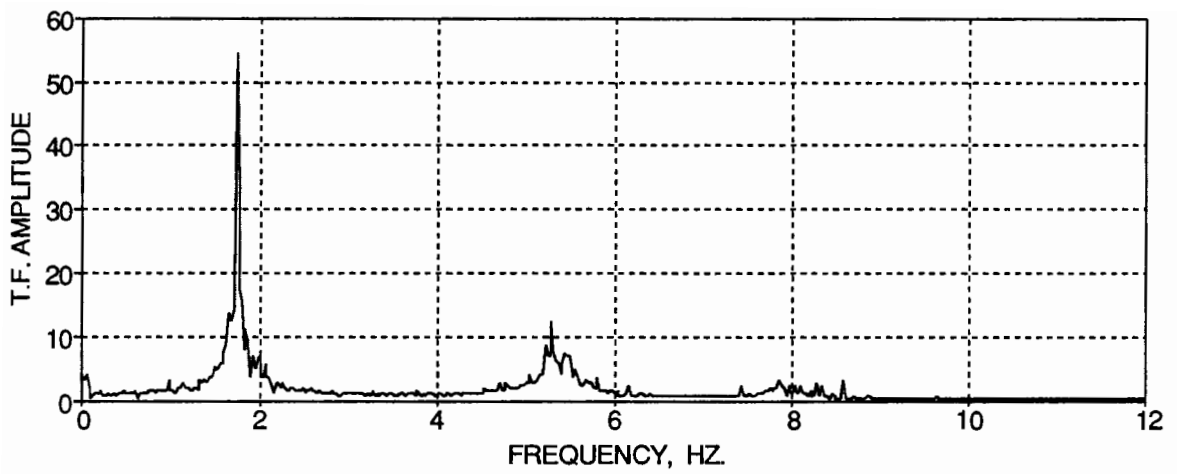

(a) Third Floor

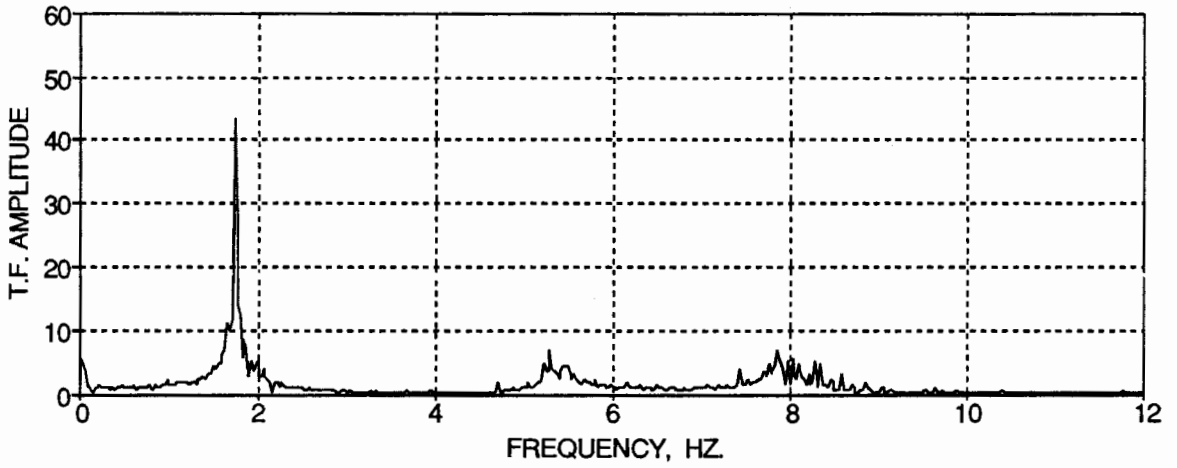

(b) Second Floor

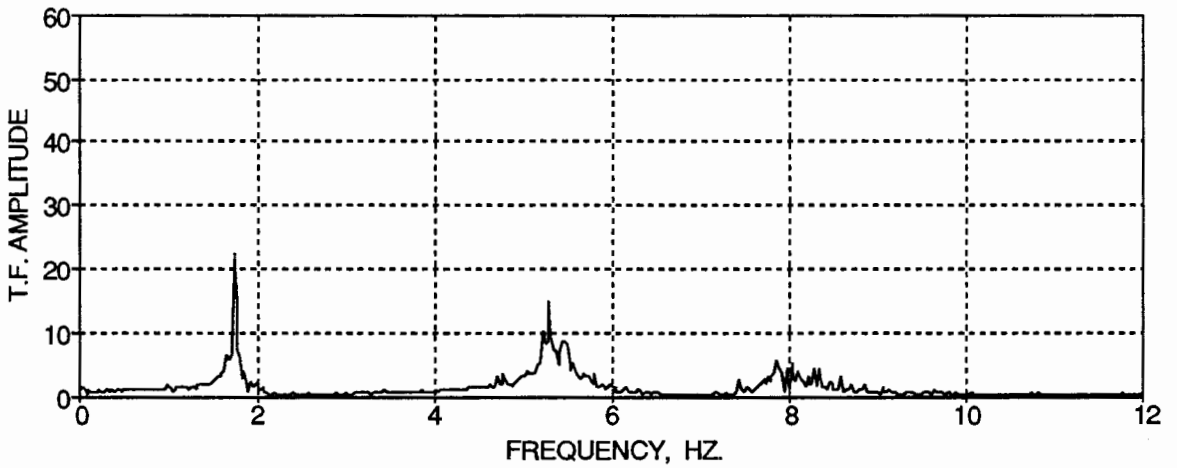

(c) First Floor

FIG. 4-11 Transfer Functions of the Story Level Accelerations from WHN_B

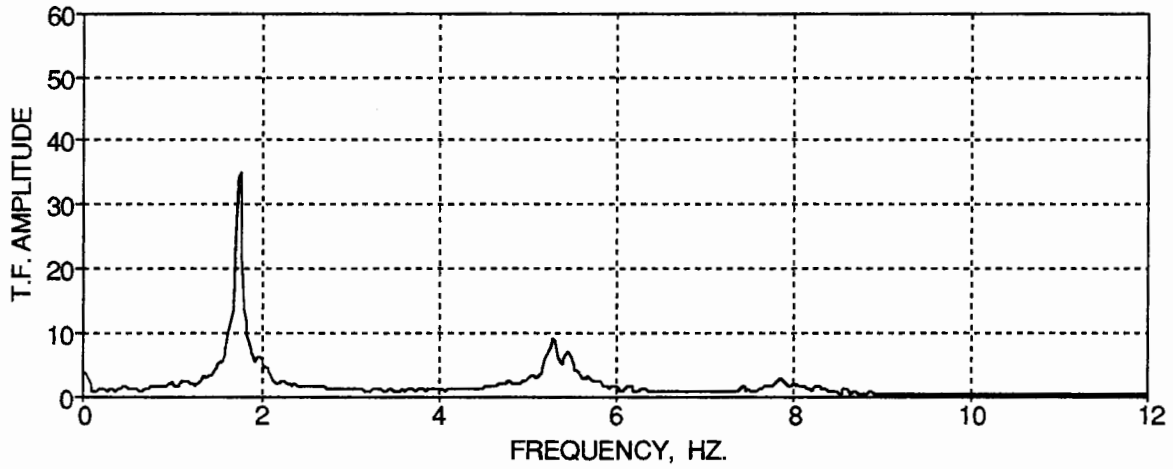

(a) Third Floor

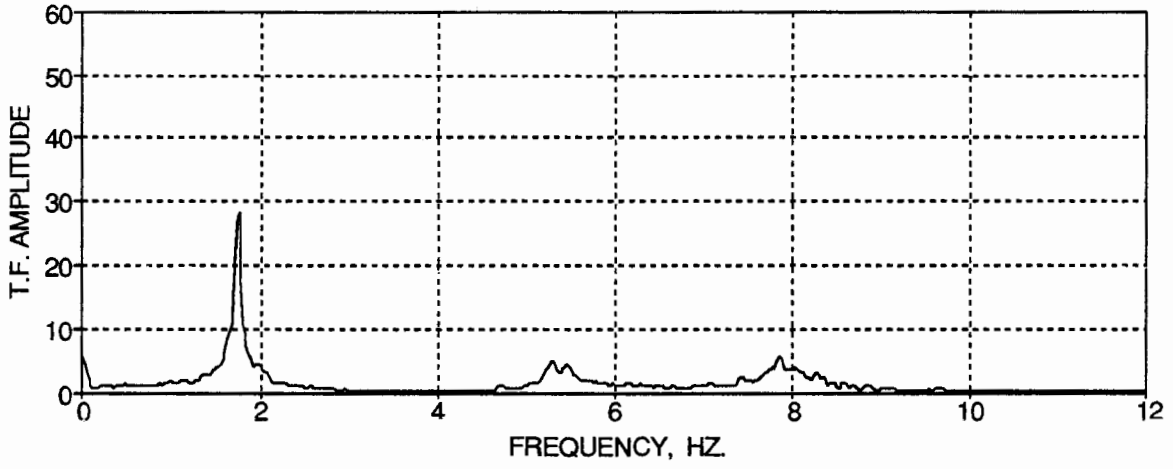

(b) Second Floor

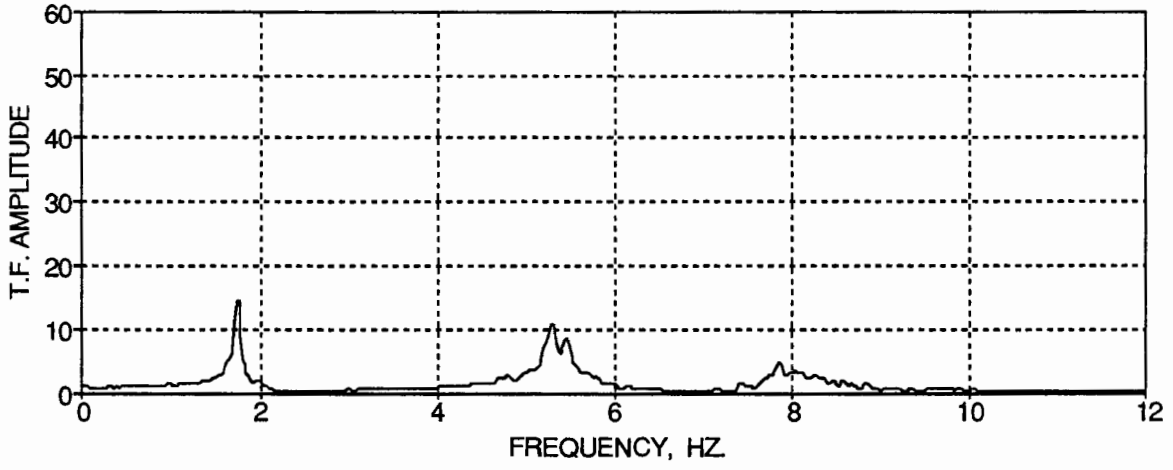

(c) First Floor

FIG. 4-12 Smoothed Transfer Functions of the Story Level Accelerations from WHN_B

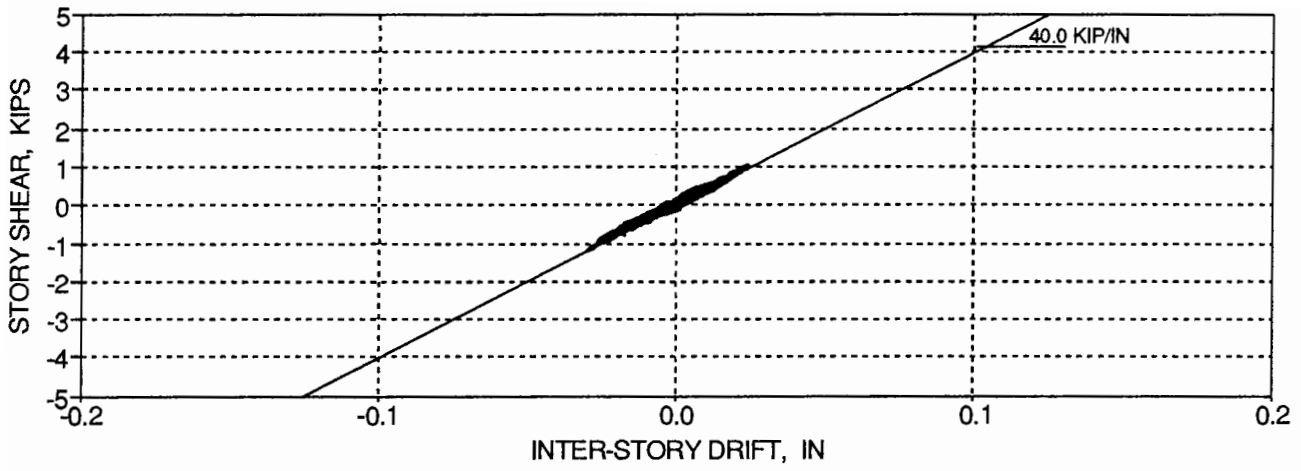

(a) Third Floor

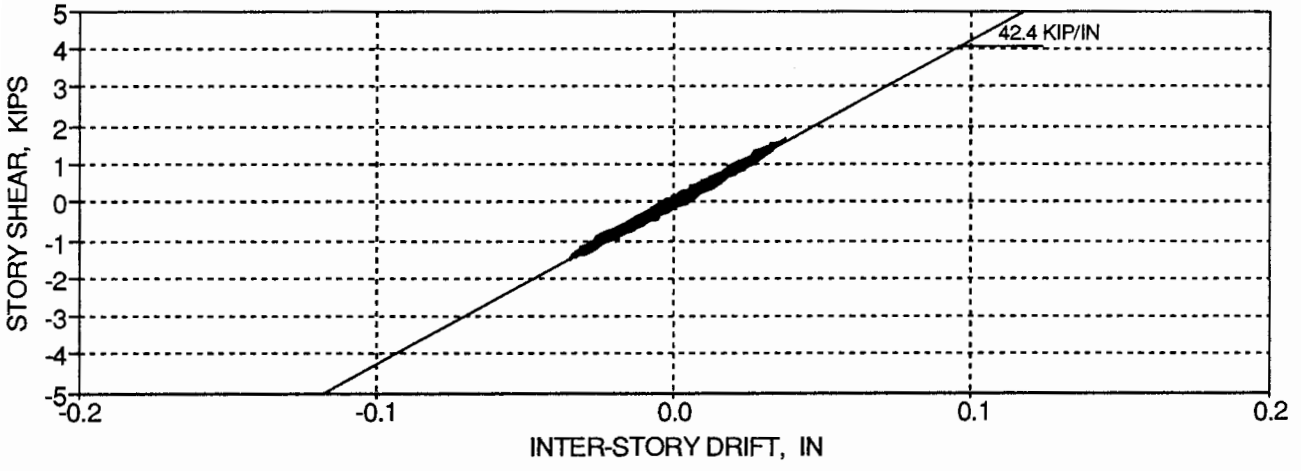

(b) Second Floor

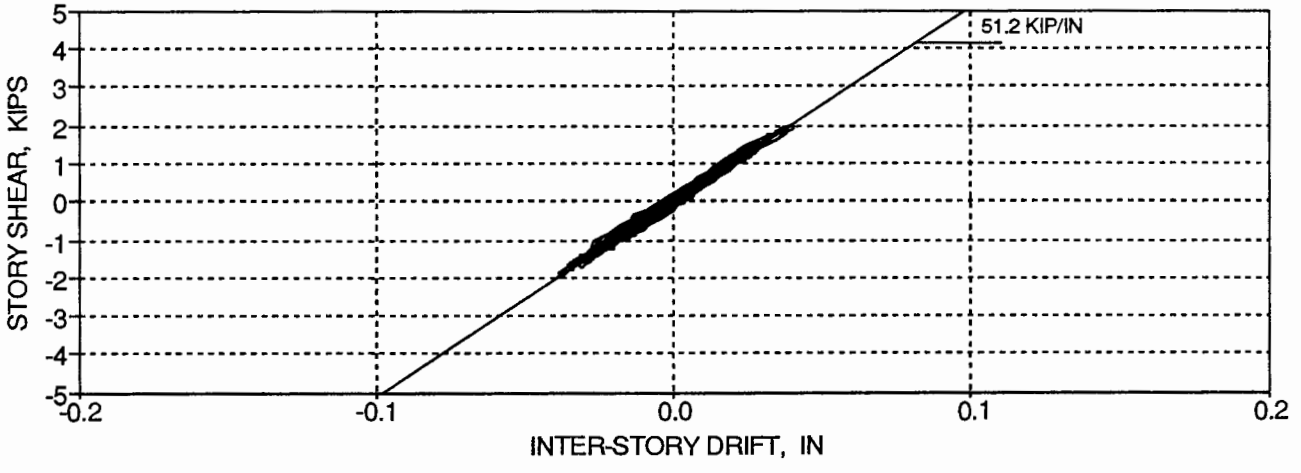

(c) First Floor

FIG 4-13 Story Shear versus Inter-Story Drift Histories for WHN_B

4.5 Analytical Identification of Dynamic Characteristics

The natural frequencies, the modal shapes, and the stiffness matrix were calculated using a dynamic analysis model (STAAD^{TM}) based on the structural member properties and their geometry. Using "full" theoretical properties for the members, a mismatch of the first mode of vibration was obtained. Therefore, the moments of inertia are modified in the computational model to fit the first mode frequency as follows:

$$(EI)_{col} = 0.565\,(EI_{col})_g \tag{4.58a}$$

$$(EI)_{beam} = 0.565\,(EI_{beam})_g \tag{4.58b}$$

where $(EI_{col})_g$ is the column stiffness based on the gross column area.

$(EI_{beam})_g$ is the beam stiffness based on the gross T-beam area with full slab contribution.

This reduction of elastic stiffness properties is required due to the micro-cracking of the model members, even in their "undamaged" state. Note that the reduction of the gross member stiffness in the beam and column members were chosen to be identical for simplicity. Although in reality, constant member stiffness reductions may not be the case since cracking or damage can be concentrated in either the beam or column members or in only certain locations of a structure.

For comparative purposes, the "fully cracked" stiffnesses of the beams and columns, determined from transformed sections, are: $(EI)_{col} = 0.23\,(EI_{col})_g$; and $(EI)_{beam} = 0.13\,(EI_{beam})_g$, respectively. Therefore the initial stiffnesses of the "undamaged" members from Eqs. (4.58a) and (4.58b) lie between the fully cracked and uncracked (gross) section properties. Similar observations were reported by El-Attar et al. (1991b) in the smaller scale test.

The natural frequencies of the unloaded model are thus calculated using the mass matrix from Eq. (4.39) and the input section properties in Eq. (4.58):

$$\mathbf{f}_i^u = \begin{pmatrix} 3.70 \\ 10.81 \\ 16.50 \end{pmatrix} \text{ Hz.} \tag{4.59}$$

The modal shape matrix of the unloaded model is determined as follows:

$$\Phi_{ij}^{u} = \begin{pmatrix} 1.00 & -0.81 & -0.43 \\ 0.78 & 0.53 & 1.00 \\ 0.40 & 1.00 & -0.88 \end{pmatrix} \tag{4.60}$$

The stiffness matrix of the unloaded model is calculated by using Eq. (4.28) with the calculated modal shapes, Eq. (4.60), and natural frequencies, Eq. (4.59), as:

$$\mathbf{K}_{ij}^{u} = \begin{pmatrix} 46.7 & -50.9 & 4.4 \\ -50.9 & 102.7 & -56.2 \\ 4.4 & -56.2 & 108.2 \end{pmatrix} \text{ kip/in} \tag{4.61}$$

The story stiffnesses of the unloaded model, defined in Eq. (4.29), are calculated from Eq. (4.61) and shown below:

$$\mathbf{k}_{i}^{u} = \begin{pmatrix} 50.9 \\ 56.2 \\ 52.0 \end{pmatrix} \text{ kip/in} \tag{4.62}$$

Likewise the natural frequencies of the loaded model are calculated from the story masses, Eq. (4.46), and the same input section properties as:

$$\mathbf{f}_{i} = \begin{pmatrix} 1.78 \\ 5.20 \\ 7.94 \end{pmatrix} \text{ Hz.} \tag{4.63}$$

The modal shape matrix of the loaded model is obtained:

$$\Phi_{ij} = \begin{pmatrix} 1.00 & -0.81 & -0.43 \\ 0.78 & 0.53 & 1.00 \\ 0.40 & 1.00 & -0.88 \end{pmatrix} \tag{4.64}$$

The stiffness matrix of the loaded model is obtained from Eq. (4.28) with the calculated modal shapes, Eq. (4.64), and natural frequencies, Eq. (4.63), as:

$$\mathbf{K}_{ij} = \begin{pmatrix} 46.7 & -50.9 & 4.4 \\ -50.9 & 102.8 & -56.3 \\ 4.4 & -56.3 & 108.2 \end{pmatrix} \text{ kip/in} \tag{4.65}$$

The story stiffnesses of the loaded model, defined in Eq. (4.29), are calculated from Eq. (4.65) and shown below:

$$\mathbf{k}_i = \begin{pmatrix} 50.9 \\ 56.3 \\ 51.9 \end{pmatrix} \text{ kip/in} \tag{4.66}$$

For representation of these analytical dynamic characteristics in the comparison, the test label of STAAD is used.

4.5.1 Comparison of Analytical and Experimental Dynamic Characteristics

Tables 4-2 and 4-3 summarize the identified natural frequencies, modal shapes, stiffness matrix, story stiffnesses, equivalent viscous damping ratios, and damping matrix of the unloaded and loaded model, respectively from the experimental identification tests and the analytical evaluation from STAAD.

(a) Unloaded Model Identification Tests

For the unloaded model, it can be observed that the identified natural frequencies from STAAD and the HAMMER test are slightly different, primarily due to the estimated quantities for the story masses, input member stiffnesses, and the small level of excitation of the higher modes from the impact hammer. Large variations in the modal shapes and stiffness matrix can be detected between the identifications of the impact hammer test and STAAD. This is again primarily attributed to the small level excitation in the higher modes with third floor strikes from the impact hammer. Only the characteristics associated with the first mode of vibration are comparable. Therefore it is concluded that the identification of the modal shapes (with exception of the first mode), stiffness matrix, story stiffnesses, and damping matrix from the impact hammer test are not reliable.

(b) Loaded Model Identification Tests

For the loaded model, comparable natural frequencies and modal shape matrices have resulted in all tests, both experimentally and analytically. It can be observed from Tables 4-2 and 4-3 that a 47.6% reduction in the first mode natural frequency (from 3.40 Hz. (HAMMER) to 1.78 Hz. (WHN_B)) occurs due to attaching the additional weights for mass similitude on the model. Similar reductions are also found in the second and third modes of vibration for the model.

Comparable stiffness matrices and story stiffnesses are observed in the PULL, WHN_B, and STAAD tests, in which the story stiffnesses are approximately equivalent for each floor. An important point to note is that the sum of the diagonal terms of the stiffness matrix of the loaded model developed analytically using STAAD corresponded to a 0.5% error compared to the results from the experimental WHN_B test for the undamaged model. Recall that the input member properties in STAAD used a reduced gross member stiffness to match the first mode natural frequency from WHN_B. Since excellent correlation exists between STAAD™ and the experimental characteristics, STAAD™ is used in the following tests to evaluate the stiffness matrix and story stiffnesses based on the correlation of the experimentally observed first mode natural frequency from the previous white noise excitation.

The identification of the first mode equivalent viscous damping factor is also comparable for each test performed. But variations of the second and third mode damping factors are observed among the various tests. Since a smoothing technique was required for both the SNAP and WHN_B tests, deviations of the higher-order damping factors are expected. Also the damping factor identification from Eq. (4.19) is based on an elastic system, which may be invalid since cracking may have developed in some of the members.

The identified viscous damping matrices of the unloaded and loaded models from the HAMMER and WHN_B tests, respectively are also shown to have large variations. But again since the damping matrix is developed from the modal shapes [see Eq. (4.30)], the determination of the damping matrix from the impact hammer test can be regarded as inaccurate.

Therefore from the above comparisons, it is concluded that the white noise identification test provides an accurate evaluation of the dynamic characteristics of the model. Thus herein only white noise excitations are used to update the dynamic characteristics of the model after an induced base motion. It is also concluded that accurate predictions of the dynamic characteristics

and stiffness matrix of the undamaged model are achieved with STAAD^{TM} using a 56.5% reduction in the gross member stiffness properties for correlating the first mode natural frequency.

Table 4-2 Dynamic Characteristics of the Unloaded Model

Test	$\mathbf{f}_i^u$ (Hz.)	$\mathbf{\Phi}_{ij}^u$	$\mathbf{K}_{ij}^u$ (kip/in)	$\mathbf{k}_i^u$ (kip/in)	ξ_i^u (%)	$\mathbf{C}_{ij}^u$
HAMMER	$\begin{pmatrix}3.40\\11.00\\17.60\end{pmatrix}$	$\begin{pmatrix}1.00 & -0.67 & -0.62\\0.82 & 0.18 & 1.00\\0.47 & 1.00 & -0.63\end{pmatrix}$	$\begin{pmatrix}70.1 & -72.1 & 10.3\\-72.1 & 115.5 & -59.2\\10.3 & -59.2 & 97.3\end{pmatrix}$	$\begin{pmatrix}72.1\\59.2\\38.1\end{pmatrix}$	$\begin{pmatrix}2.7\\1.5\\1.0\end{pmatrix}$	$\begin{pmatrix}0.028 & -0.007 & -0.003\\-0.007 & 0.028 & -0.005\\-0.003 & -0.005 & 0.033\end{pmatrix}$
STAAD (0.565 EI_g)	$\begin{pmatrix}3.70\\10.81\\16.50\end{pmatrix}$	$\begin{pmatrix}1.00 & -0.81 & -0.43\\0.78 & 0.53 & 1.00\\0.40 & 1.00 & -0.88\end{pmatrix}$	$\begin{pmatrix}46.7 & -50.9 & 4.4\\-50.9 & 102.7 & -56.2\\4.4 & -56.2 & 108.2\end{pmatrix}$	$\begin{pmatrix}50.9\\56.2\\52.0\end{pmatrix}$	-	-

Table 4-3 Dynamic Characteristics of the Loaded Model

Test	$\mathbf{f}_i$ (Hz.)	$\mathbf{\Phi}_{ij}$	$\mathbf{K}_{ij}$ (kip/in)	$\mathbf{k}_i$ (kip/in)	ξ_i (%)	$\mathbf{C}_{ij}$
PULL	$\begin{pmatrix}1.76\\5.34\\8.15\end{pmatrix}$	$\begin{pmatrix}1.00 & -0.82 & -0.41\\0.76 & 0.55 & 1.00\\0.40 & 1.00 & -0.88\end{pmatrix}$	$\begin{pmatrix}47.4 & -52.7 & 3.2\\-52.7 & 109.3 & -59.8\\3.2 & -59.8 & 113.9\end{pmatrix}$	$\begin{pmatrix}52.7\\59.8\\54.1\end{pmatrix}$	-	-
SNAP	$\begin{pmatrix}1.86\\5.66\\8.40\end{pmatrix}$	-	-	-	$\begin{pmatrix}2.5\\4.8\\4.0\end{pmatrix}$	-
WHN_B (Eq.(4.20))	$\begin{pmatrix}1.78\\5.32\\7.89\end{pmatrix}$	$\begin{pmatrix}1.00 & -0.82 & -0.46\\0.80 & 0.46 & 1.00\\0.42 & 1.00 & -0.83\end{pmatrix}$	$\begin{pmatrix}51.9 & -53.4 & 2.5\\-53.4 & 102.4 & -54.4\\2.5 & -54.4 & 104.7\end{pmatrix}$	$\begin{pmatrix}53.4\\54.4\\50.3\end{pmatrix}$	$\begin{pmatrix}2.0\\2.4\\2.0\end{pmatrix}$	$\begin{pmatrix}0.072 & -0.042 & -0.012\\-0.042 & 0.097 & -0.029\\-0.012 & -0.029 & 0.112\end{pmatrix}$
WHN_B (Eq.(4.19))	-	-	-	-	$\begin{pmatrix}1.7\\1.6\\1.4\end{pmatrix}$	-
STAAD (0.565 EI_g)	$\begin{pmatrix}1.78\\5.20\\7.94\end{pmatrix}$	$\begin{pmatrix}1.00 & -0.81 & -0.43\\0.78 & 0.53 & 1.00\\0.40 & 1.00 & -0.88\end{pmatrix}$	$\begin{pmatrix}46.7 & -50.9 & 4.4\\-50.9 & 102.8 & -56.3\\4.4 & -56.3 & 108.2\end{pmatrix}$	$\begin{pmatrix}50.9\\56.3\\51.9\end{pmatrix}$	-	-